Lund University

Master Thesis

A Theoretical Investigation of Thermoelectrics in Nanowires Embedded With a Quantum Dot Superlattice

Author:
John Lovén

Supervisor:
Martin Leijnse

Examinator:
Carina Fasth

A thesis submitted in fulfilment of the requirements for the degree of Master of Science in Engineering

in the

Thermoelectricity Research Group
Solid State Physics

June 2015

"There is nothing as practical as a good theory."

Kurt Lewin

LUND UNIVERSITY

Abstract

Faculty of Engineering
Solid State Physics

Master of Science in Engineering

A Theoretical Investigation of Thermoelectrics in Nanowires Embedded With a Quantum Dot Superlattice

by John Lovén

Thermoelectric elements have long been anticipated to challenge conventional solutions for converting heat to electricity. However, the revolution has been stalled due to the inability to reach efficiencies comparable to their conventional counterparts, while retaining a high output power. In this work we will model a thermoelectric element based on nanowires embedded with a quantum dot superlattice using a transport model dependent on coherent transport of electrons, and show that it is theoretically possible to both increase the output power as well as reach an efficiency close to the theoretical maximum limit.

Thanks

to Martin, my supervisor, for your enthusiasm and support along the way, and your ability to bring yourself down to a master student's level of understanding: a skill rarely seen among experienced researchers.

to the Thermoelectrics Research Group, for great input along the way.

to the Condensed Matter Theory Research Group, for even greater input along the way.

to Andreas, for name-dropping effects studied in your previous works, which in turn became a large part of my work.

to Martin, my dear quantum companion, for interesting discussions and endless movie quizzes, and for making me choose to study physics in the first place.

Contents

Physical Constants

Boltzmann's constant		k_B	=	$1.380\ 65 \times 10^{-23}$	[JK^{-1}]
Electron affinity	(InAs)	χ_{InAs}	=	4.92	[eV]
...	(InP)	χ_{InP}	=	4.38	[eV]
Electron mass	(free)	m_0	=	$9.109\ 382\ 91 \times 10^{-31}$	[kg]
...	(InAs)	m_{InAs}	=	$m_0 \times 0.022$	[kg]
...	(InP)	m_{InP}	=	$m_0 \times 0.08$	[kg]
Elementary charge		e	=	$1.602\ 176\ 57 \times 10^{-19}$	[C]
Planck's constant		h	=	$6.626\ 1 \times 10^{-34}$	[Js]
Reduced Planck's constant		$\hbar$	=	$h/2\pi$	[Js]

Chapter 1

Introduction

In the year 1821, Thomas Johann Seebeck discovered that when externally short-circuiting two coupled dissimilar metals whose junctions are at different temperature, and holding a compass needle over it, the needle will deflect [1, 2]. The reason for this was later discovered to be the occurrence of a magnetic field induced by a current through the metal interface as a result of the temperature difference between the junctions. More specifically, the temperature difference gives rise to a voltage difference, something that is today known as the *Seebeck effect*. This voltage difference can in turn be used to drive a current. Ever since then, there have been attempts to construct thermoelectric elements that make use of this effect, in order to extract energy from a temperature difference. Conventionally, many of these thermoelectric elements are combined into a *thermocouple* consisting of n-type and p-type semiconductors. These are connected electrically in series and thermally in parallel, in order to increase the operating voltage [3].

The potential advantages of using thermoelectric elements over conventional electrical generators are many. For one thing, such a system consists of no moving parts, meaning less risk of it breaking. It could also enable energy conversion using heat that would otherwise be to no use, such as the waste heat produced by a combustion engine.

Instead of using the thermoelectric element as a heat engine it is also possible to do the opposite by driving a current through the element, and use it as a cooling element to further increase a temperature difference. This is known as the *Peltier effect* and could be used for local cooling in electronic devices, or even in biological tissue [4].

However, thermoelectric element based heat converters have yet to challenge their conventional counterparts, due to an inability to reach a comparable output power and efficiency. A parameter related to the efficiency of a thermoelectric device that is often

used is the so called *figure of merit ZT* and much effort has been made to increase this, e.g. by increasing the open circuit voltage called the *thermopower*, increasing the electrical conductivity, or decreasing the thermal conductivity. .

This work will be dedicated to modelling thermoelectric elements based on nanowires embedded with a quantum dot superlattice, in order to theoretically investigate the possibility to enhance both the output power as well as the efficiency.

But let's start at the beginning, by describing some of the physics behind thermoelectricity, as well as motivating why these superlattice structures are of interest in the first place.

1.1 The Seebeck effect

Consider Figure 1.1. The electrons in a solid material with a finite temperature will have a certain energy spread and the higher the temperature, the larger the spread. This energy distribution follows the so called *Fermi distribution* $f(E)$ and can in the figure be seen for two different temperatures. The *Fermi level*, that is the energy level with a 50% probability of being occupied by an electron, is marked with a dashed line, and is the same in both temperature cases.

In 3D, the *density of states* (DOS) for the electrons in the material increases with the square root of the energy, meaning there are more energy levels at higher energies, as can be seen in the centre of the figure.

Worth mentioning is that electrons with higher energy will also have a higher velocity, leading to more electrical current being transmitted through electrons with higher energy.

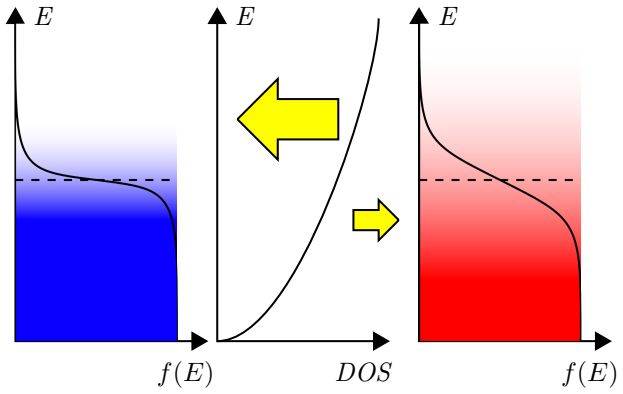

FIGURE 1.1: Schematic illustrating the thermoelectric effect in 3D.

Now let's consider the two Fermi distributions in the figure describing the electron energy spread in the two ends of the same conductor. If we keep the system out of thermal equilibrium and maintain the temperature difference between the two ends, e.g. by connecting them to different heat sinks, we will have a net diffusion current of electrons moving from the hot to the cold end. If open circuited, this will lead to an accumulation of electrons at the cold end which will give rise to a voltage difference, and this is commonly known as the Seebeck effect. This voltage difference can in turn be used to extract energy from the system.

1.2 Room for improvement

From an energy harvesting point of view, there are a few obvious drawbacks to the system described in the previous section.

One is that all electrons with an energy below the Fermi level give rise to a current going in the wrong direction, illustrated in Figure 1.1 with the small arrow of current, which will decrease the net current and hence also the possible *power output* from such a device.

Another disadvantage has to do with the high energy electrons that carry current. All electrons carry the same amount of electrical current, due to the electron elementary charge being quantized. But electrons with higher energy carry a larger *heat current*, as they have an energy further from the Fermi energy. Hence high energy electrons that are part of the transport will lead to a decrease in the device *efficiency*.

Optimally we therefore want no electron transmission below the Fermi level, and the current above the Fermi level to be carried by electrons as close to the Fermi energy as possible.

1.3 Lowering the dimensions

By making the conductor between the two heat sinks radially very thin, we lower the dimensions of the conductor from 3D to 1D. This has been anticipated to significantly increase the figure of merit ZT [5, 6].

In 1D, the density of states is proportional to one over the square root of energy, hence there are more electrons with lower energy. As mentioned in the previous section this is advantageous, since it will lower the amount of higher energy electrons that carry current.

But this does not change the fact that we still have electron transmission below the Fermi level, carrying current in the wrong direction. For this we need a way to selectively choose what the electron energy must be in order for the electron to be allowed to be transmitted through the device.

1.4 Using quantum dot embedded nanowires

Nanowires (NWs) are thin elongated semiconductor cylinders[1]. Since the diameter of the NW is so small (20-200 nm) it can be seen as having only one dimension, hence we fulfil the requirements described in the previous section of having a density of states in 1D.

NWs are conventionally grown using the bottom-up approach in its axial direction, and it is possible to make abrupt changes in the semiconductor material during growth [7]. This makes it possible to embed *quantum dots (QDs)* inside the nanowire [8]. Due to resonant tunnelling through the QDs they act as energy filters, allowing only electrons of specific energies to be transmitted through the structure.

By engineering a QD embedded NW, and doping or gating the leads on either side of the QD structure to place the Fermi level at an appropriate position, it is possible to force the structure to only transmit electrons with energies above the Fermi level in a very well defined interval. By only allowing transport close to the Fermi level it is possible to achieve quite high efficiencies, since the electrons carry very little heat.

The problem with this is that, because the QD gives rise to a very narrow energy interval in which the electrons are allowed to be transmitted through the structure, the current and hence also the power output from such a device is very small. Also, the transmission peaks resulting from the resonant tunnelling through a single QD follow the smooth shape of a *Lorentzian distribution*, which is not optimal for achieving a high efficiency.

1.5 Combining QDs into a superlattice

It has been shown that in order to maximize the efficiency of a thermoelectric element given a certain power output, the *transmission function* describing the probability of transmission for electrons as a function of energy, needs to have a rectangular shape [9].

[1]Nanowires do not necessarily have be cylindrical, but this will be neglected since we in this project will disregard the shape and dimension of the nanowire cross-section.

This means that in a certain energy interval, all electrons will be transmitted through the structure. Outside this interval, no electrons will be transmitted.

A suggestion of how to realize this transmission function is to connect several QDs in series to form a so called *superlattice*. Similar to when atoms are clustered together and their discrete energy levels split into energy bands, the peaks in the transmission function related to the energy levels of a single QD split into several adjacent peaks when connected in series.

This approach seems promising in order to engineer the rectangular transmission function needed to maximize the efficiency of such a thermoelectric device and has also been tested experimentally [10]. Several methods exist for calculating the heat and charge currents, including using Non-Equilibrium Green's Functions [11], master equations [12], and Boltzmann equations [13].

In this work, we will utilize the power of *T-matrices*, that relies on coherent elastic scattering in a potential structure consisting of potential barriers with finite dimensions, in order to calculate the transmission function used when calculating the currents [14, p. 153-162].

1.6 Goals

The main goal of this project is to theoretically investigate the thermoeletric properties of a NW embedded with a superlattice of QDs. In particular it is of interest to compare these results to those of a NW embedded with a single QD. The hope is to be able to show that the output power will increase while still retaining a high efficiency.

To achieve this goal, much effort will be put into engineering a rectangular transmission function, calculated using T-matrices, by optimizing different parameters of the NW's conduction band potential structure.

Chapter 2

Theory

2.1 Model

A schematic of the device that will be modelled is shown in Figure 2.1, and is an illustrative representation of a NW contacted at both ends.

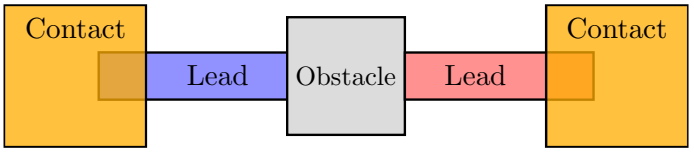

FIGURE 2.1: Schematic of the theoretical setup of the device that is modelled.

The model and the methods used in the project will be summarized in this section and described in greater detail later in this chapter.

2.1.1 Scattering

The NW contains an embedded structure in its centre called an *obstacle* which is the only scattering centre for electrons travelling through the device. Hence there is no scattering in the interface between the leads and the contacts. This obstacle can be e.g. an energy barrier or a QD, and will be modelled as a specified potential structure representing the lower conduction band edge. Depending on what this potential structure looks like, it will selectively reflect and transmit electrons depending of their energy. The transmission probability for a certain electron energy will be given by the transmission function, which is calculated using *T-matrices*. We deal only with elastic scattering

events, and throughout the obstacle and its contactation to the leads, the electrons have constant energy.

2.1.2 Potential structure

The potential structure of the lower conduction band edge will be modelled as alternating layers of indium arsenide (InAs) and indium arsenide phosphide ($InAs_{1-x}P_x$). Varying the amount of phosphorus will in turn vary the structure potential and make it possible to construct energy barriers of different heights. A change in material composition will also result in a different effective electron mass in that segment of the NW.

2.1.3 Dimensionality

The electron *wave function* is, due to the small radial dimension of the NW, approximated to having only 1 dimension, hence the electron energy is only dependent on the *wave vector* k in the axial direction.

2.1.4 Temperature

A temperature difference is set between the two leads on either side of the obstacle, and results in a smearing of the two Fermi distributions.

We will consider one low and one high temperature regime: 4 K – 10 K and 250 K – 300 K for the cold – hot lead respectively. The low temperature regime is chosen because it is a common temperature for doing experimental testing on nano sized thermoelectric elements. The high temperature regime is chosen because it is around room temperature, and hence relevant for energy harvesting in practice.

2.1.5 Heat transport

When calculating the heat loss, we limit ourselves to the heat carried by the electrons, and neglect all other sorts of heat transfer such as phonon transport or heat lost to the surroundings.

2.1.6 Current

Both electrical current and heat current is calculated using *Landauer formalism*.

2.1.7 Voltage bias

The voltage bias we put over the NW in order to model the power extraction is modelled as a shifting of the Fermi levels in the leads.

2.2 Electron wave function

In this project, we will look at the electron as a propagating wave, described by a wave function. The wave function is obtained by solving the time-independent *Schrödinger equation* for the two leads on either side of the obstacle mentioned in Section 2.1.

Because we work with NWs, that are thin elongated cylinders, the medium in which the electrons travel can be seen as having only 1 dimension: along the z-axis of the NW. In the other two dimensions the electron is confined due to the small radius of the NW. The solution to the Schrödinger equation for a free electron in the NW lead will then be

$$\Psi_n(x,y)\Psi(z) = \Psi_n(x,y)(Ae^{ik_z z} + Be^{-ik_z z}), \tag{2.1}$$

where

$$k_z = \sqrt{\frac{2m(E-V_0)}{\hbar}} \equiv k, \tag{2.2}$$

is the electron wave number along the NW axis, E the electron energy, V_0 the potential, and m the effective mass of the electron, which depends on the material it is travelling in.

As can be seen in Eq. (2.1), $\Psi(z)$ consist of two partial waves travelling in opposite directions along the NW axis. It can also be seen that the total wave function will have a term $\Psi_n(x,y)$ which will be standing waves dependent on the dimensions of the NW cross-section. Since we neglect the dimensions of the cross-section, and because there is transport only in the z-direction along the NW, we will ignore these terms. The eigen energies of these terms will however result in different *sub-bands*, and will lead to an energy shift of the lower edge of the conduction band. We will only look at the sub-band with the lowest energy, and define the lower edge of the conduction band in the leads to be at zero potential.

2.3 Transmission function

The transmission function *T(E)* gives the probability for an electron of energy E to be transmitted through a specified potential structure, and we will now go through how to calculate it.

As can be seen in Eq. (2.1) the solution to the Schrödinger equation will depend on the wave vector k of the electron, and Eq. (2.2) shows that k is dependent on the effective electron mass as well as its kinetic energy. A change in material along the NW will change both of these parameters, meaning the electron wave functions on either side of such a material interface must be different. We will henceforth call this interface a *step*.

2.3.1 Modelling the transition through a step

Shown in Fig. 2.2 is an illustration of a potential step inside the structure along the NW axis.

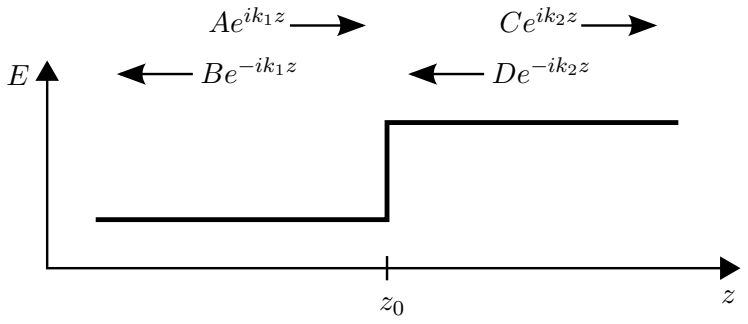

FIGURE 2.2: Illustration of the potential structure for a single step, e.g. an interface between two different materials.

Because the potentials on either side of the obstacle differs from each other, the wave vectors k of the wave functions of electrons on either side of the obstacle must also differ, which requires two separate solutions to the Schrödinger equation according to Eq. (2.1):

$$\Psi(z) = \begin{cases} \Psi_1(z) = Ae^{ik_1z} + Be^{-ik_1z}, & z < z_0, \\ \Psi_2(z) = Ce^{ik_2z} + De^{-ik_2z}, & z > z_0. \end{cases}$$

We want the total wave function across the structure to be continuous, meaning their value must match at the interface, which yields the first boundary condition:

$$\Psi_1(z_0) = \Psi_2(z_0).$$

Furthermore, it is necessary to have current conservation for transport through the obstacle, giving a second boundary condition [14, p. 195]:

$$\frac{1}{m_1}\frac{d\Psi_1(z)}{dz}\bigg|_{z=z_0} = \frac{1}{m_2}\frac{d\Psi_2(z)}{dz}\bigg|_{z=z_0}.$$

Inserting the wave function from Eq. (2.1) into these two boundary conditions gives

$$\begin{aligned} Ae^{ik_1z_0} + Be^{-ik_1z_0} &= Ce^{ik_2z_0} + De^{-ik_2z_0}, \\ \frac{k_1}{m_1}(Ae^{ik_1z_0} - Be^{-ik_1z_0}) &= \frac{k_2}{m_2}(Ce^{ik_2z_0} - De^{-ik_2z_0}), \end{aligned}$$

and combining them yields

$$\begin{aligned} Ce^{ik_2z_0} &= \frac{\frac{k_2}{m_2}+\frac{k_1}{m_1}}{2\frac{k_2}{m_2}}Ae^{ik_1z_0} + \frac{\frac{k_2}{m_2}-\frac{k_1}{m_1}}{2\frac{k_2}{m_2}}Be^{-ik_1z_0}, \\ De^{-ik_2z_0} &= \frac{\frac{k_2}{m_2}-\frac{k_1}{m_1}}{2\frac{k_2}{m_2}}Ae^{ik_1z_0} + \frac{\frac{k_2}{m_2}+\frac{k_1}{m_1}}{2\frac{k_2}{m_2}}Be^{-ik_1z_0}. \end{aligned}$$

These two equations can be written in matrix form, and after some rearrangements we get

$$\begin{aligned} \begin{pmatrix} C \\ D \end{pmatrix} &= \begin{pmatrix} e^{-ik_2z_0} & 0 \\ 0 & e^{ik_2z_0} \end{pmatrix} \frac{1}{2k_2m_1} \begin{pmatrix} k_2m_1+k_1m_2 & k_2m_1-k_1m_2 \\ k_2m_1-k_1m_2 & k_2m_1+k_1m_2 \end{pmatrix} \begin{pmatrix} e^{ik_1z_0} & 0 \\ 0 & e^{-ik_1z_0} \end{pmatrix} \begin{pmatrix} A \\ B \end{pmatrix} \\ &\equiv M_s(z_0)\begin{pmatrix} A \\ B \end{pmatrix}. \end{aligned}$$

where $M_s(z_0)$ is denoted the *step transfer matrix*, and connects the amplitude of the wave functions on either side of the potential step at position $z = z_0$ in the potential structure. Note that $M_s(z_0)$ can, depending on the matrix parameters, represent both a step up and a step down in potential.

2.3.2 Combining transfer matrices

To model a more complex structure, such as that of a double barrier QD shown in Fig 2.3, we need to combine multiple step transfer matrices, or T-matrices, described in the previous section. Since the outgoing wave from one step is the ingoing wave to the next, this is done by simply multiplying the T-matrices for different steps in the right order.

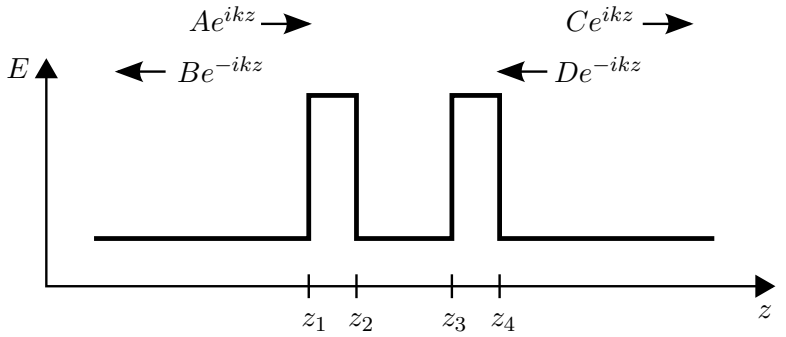

FIGURE 2.3: Illustration of the potential structure for a double barrier QD.

For the structure shown in Fig. 2.3 we multiply the ingoing wave amplitudes with T-matrices in the following order:

$$\begin{aligned} \begin{pmatrix} C \\ D \end{pmatrix} &= M_{s-}(z_4)M_{s+}(z_3)M_{s-}(z_2)M_{s+}(z_1)\begin{pmatrix} A \\ B \end{pmatrix} \\ &\equiv M\begin{pmatrix} A \\ B \end{pmatrix}, \end{aligned}$$

where $M_{s+}(z)$ and $M_{s-}(z)$ represent a step up and a step down in potential, respectively, and M is the total transfer matrix of the potential structure.

If we approximate all material transitions in the NW to be represented as abrupt shifts in the potential structure, we can use combined T-matrices to model the electron transmission through an arbitrary structure.

2.3.3 Wave amplitude and transmission flux

Consider the functions in Fig. 2.2 or 2.3 and an electron hitting the obstacle from the left. Because of this impact direction we define the right going wave on the left side to have an amplitude equal to 1, hence $A = 1$. For the same reason we have no left going wave from the right, so $D = 0$. The right going wave on the right is the one that has been transmitted through the structure and we therefore denote its amplitude $C = t$. Lastly, the left going wave on the left is what is being reflected back from the structure, so we denote its amplitude $B = r$.

We are only interested in what is being transmitted through the structure, and we get the amplitude of the transmitted wave using

$$\begin{pmatrix} C \\ D \end{pmatrix} = M \begin{pmatrix} A \\ B \end{pmatrix}, \quad \Rightarrow \quad \begin{pmatrix} t \\ 0 \end{pmatrix} = \begin{pmatrix} M_{11} & M_{12} \\ M_{21} & M_{22} \end{pmatrix} \begin{pmatrix} 1 \\ r \end{pmatrix} = \begin{pmatrix} M_{11} + M_{12}r \\ M_{21} + M_{22}r \end{pmatrix}, \quad \Rightarrow$$

$$\left.\begin{aligned} t &= M_{11} + M_{12}r \\ 0 &= M_{21} + M_{22}r \end{aligned}\right\}, \quad \Rightarrow \quad t = \frac{M_{11}M_{22} - M_{12}M_{21}}{M_{22}}.$$

Hence we can calculate the amplitude of the transmitted wave by only using the elements of the total T-matrix.

So far we have been looking on the transmission of the wave amplitudes. But what we are really interested in is the *transmission flux* T of the potential structure.

A wave Ae^{ikx} carries a number current density $\frac{\hbar k}{m}|A|^2$. The flux transmission through an obstacle is calculated by taking the ratio between the transmitted and incident current density.

Combining these facts with the amplitude coefficients previously retrieved in this section, we get the transmission flux

$$T(E) = \frac{\frac{\hbar k_2}{m_2}|t|^2}{\frac{\hbar k_1}{m_1}|1|^2} = \frac{k_2 m_1}{k_1 m_2}|t|^2.$$

When the material in the two leads are the same, this expression simplifies to

$$T(E) = |t|^2,$$

This is our transmission function, which will depend on the energy E of the electron as well as the properties of the potential structure.

2.4 Material composition

As mentioned in Sec. 2.1, the effective electron mass will depend on which material the electron is travelling in. All sections of the structure with zero potential will be modelled as InAs, and the electrons in these sections to have the corresponding effective electron mass.

To make a structure with non-zero potential we model a composition of $InAs_{1-x}P_x$. Changing the amount of phosphorus will in turn change the structure potential.

Assuming that the effective electron mass $m(x)$ for $InAs_{1-x}P_x$ is linearly dependent on the amount x of phosphorus in the composition, with $m(0) = m_{InAs}$ and $m(1) = m_{InP}$, we can calculate the effective electron mass

$$m_{InAs_{1-x}P_x} = m_{InAs} + x(m_{InP} - m_{InAs}),$$

$$0 \leq x \leq 1.$$

Changing the amount x of phosphor will also change the conduction band edge and hence the structure potential. If we assume that the difference in potential ΔE between two materials is equal to the difference between the corresponding electron affinity in the materials, and that the electron affinity $\chi(x)$ for $InAs_{1-x}P_x$ is linearly dependent on the amount of phosphor x in the composition, with $\chi(0) = \chi_{InAs}$ and $\chi(1) = \chi_{InP}$, we can calculate the structure potential:

$$\Delta E = x(\chi_{InAs} - \chi_{InP}),$$

$$0 \leq x \leq 1.$$

2.5 Fermi distribution

As mentioned in Sec. 1.1, the Fermi distribution describes the energy spread of the electrons in the leads, and is calculated using the expression

$$f(E, \mu) = \frac{1}{1 + e^{(E - \mu)/k_B T}},$$

with k_B being *Boltzmann's constant*, μ the Fermi level and T the temperature in the lead.

More precisely, the Fermi distribution describes the probability that an energy level at energy E is being occupied by an electron, and the Fermi distribution for different temperatures can be seen in Fig. 2.4.

It is clear that a higher temperature leads to a higher spread of electron energies. The reason for this is that electrons with lower energy can get thermally excited to a higher energy level.

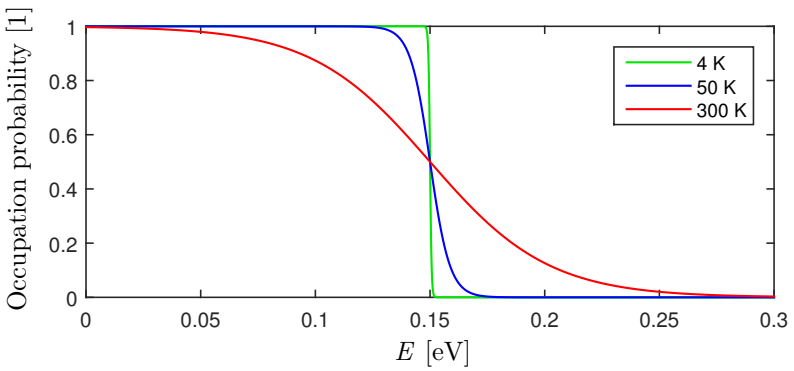

FIGURE 2.4: Fermi distributions for different temperatures with the Fermi level set to 0.15 eV.

As mentioned in Sec. 2.1, a voltage difference between the leads will be modelled by a shifting of the Fermi levels in the leads. More precisely, we decide that a voltage V_{bias}, which will be described in Sec. 2.7, leads to a shift

$$\Delta\mu = \frac{eV_{bias}}{2},$$

up in the cold lead and down in the hot lead.

In Sec. 2.6 we will go through how to calculate the current through the device. As can be seen in Eq. (2.3), the current is dependent on the difference between the Fermi distributions in the two leads. This difference for different bias voltages in the two different temperature regimes is shown in Fig. 2.5.

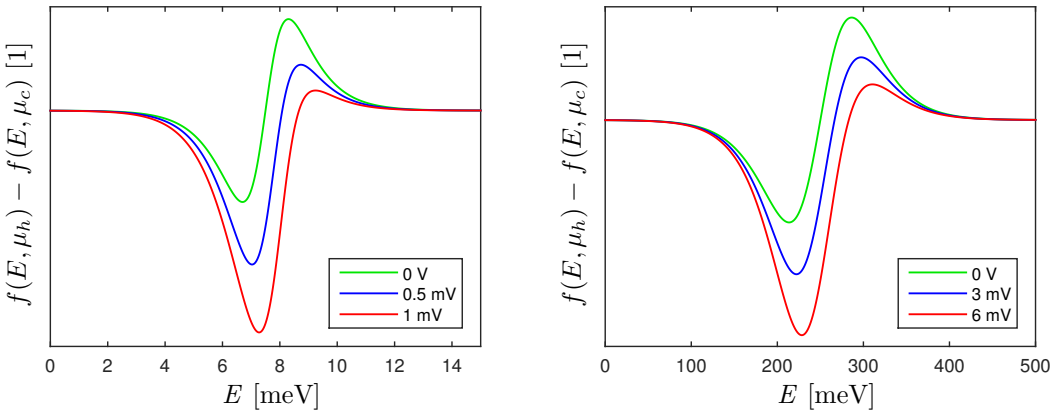

(A) 4 K and 10 K.

(B) 250 K and 300 K.

FIGURE 2.5: The difference between the Fermi distributions in (A) the cold and (B) hot temperature regime, at different bias voltages.

Without bias, the Fermi level is set to the middle of the graphs. When a bias is applied, the Fermi energies will shift as previously described.

The graph can be seen as an indication of how many electrons at a specific energy will be transported from the hot to the cold lead, due to a higher concentration of electrons at this energy in the hot lead. Hence at energies for which the graph is above zero there will be a net electron current going from hot to cold, which is what we want. The part of the graph that lies below zero will as mentioned in 1.2 lead to a current in the wrong direction, from cold to hot. We see that as we increase the bias, this part of the graph will become more significant.

As will be seen in Eq. (2.3), the difference between the leads' Fermi functions is multiplied with the transmission function in order to get the current. By engineering a selective transmission function in the form of a rectangle, we can in theory completely remove the influence of the parts of the graphs in Fig. 2.5 where they go below zero.

2.6 Electrical current

Because we deal with electronics, we need a method for calculating the current through our device. The way we chose to do the modelling described in Section 2.1 enables us to calculate the current using *Landauer formalism*.

The expression for calculating the current in 1D will then be [14, p. 164]

$$I = \frac{2e}{h} \int_{E_{C_c}}^{\infty} (f(E, \mu_c) - f(E, \mu_h)) T(E) dE, \tag{2.3}$$

where $f(E, \mu)$ is the Fermi distribution for the two leads described in the previous section, e is the elemental charge of one electron to change the expression from particle current to charge current, the 2 is to account for spin, h is *Planck's constant* and $T(E)$ is the transmission function of the obstacle described in Sec. 2.3. We perform the integration from the bottom edge of the conduction band in the cold lead to infinity.

Generally the current will also depend on the velocity of the electrons as well as the density of states. In 1D however, the density of states precisely cancels out the energy dependence of the velocity.

In 3D however, the electron density of states has to be taken into account. Because we now deal with more than 1 dimension, we need to instead use an expression for calculating the current density J using [14, p. 166]

$$J = \frac{e}{h} \int_{E_{C_c}}^{\infty} (n_{2D}(E, \mu_c) - n_{2D}(E, \mu_h)) T(E) dE, \tag{2.4}$$

where

$$n_{2D}(E,\mu) = \frac{mk_BT}{\pi\hbar^2}\ln(1+e^{(\mu - E)/kT}),$$

is the density of electrons in the two-dimensional xy-plane, with kinetic energy $E = \frac{\hbar^2k^2}{2m}$ due to motion in the z-direction. Eq. (2.4) will only be used to be able to compare the 1D and 3D case.

2.7 Power

In order to extract power from the device we need to connect both ends over a load resistance. This will give rise to a voltage drop over the load which multiplied with the current through the load gives the output power as shown in Figure 2.6A.

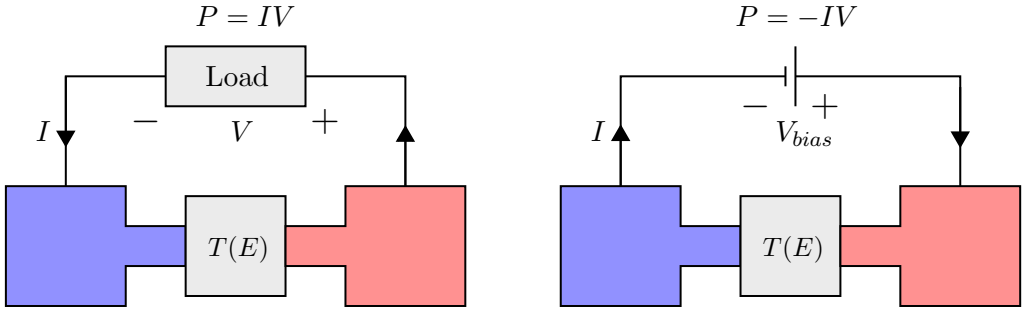

(A) How the power extraction works. (B) How we model the power extraction.

FIGURE 2.6: Schematic (A) of how we extract power from the device, and (B) how we model it.

To model this we simply calculate the *I-V characteristics* of the device by applying a voltage over the device in the same direction the voltage drop over the load would be, as shown in Figure 2.6B, and the power output will then be

$$P = -IV.$$

The minus sign is there because the direction in which we define the current to be positive, according to Figure 2.6B.

If we find a bias voltage that gives a desired output power, we can then simply calculate which load resistance gives that voltage drop, and put that into the circuit of our real device.

2.8 Efficiency and heat current

Apart from the power output we also want to be able to calculate the *efficiency* of the device, and for that we need to know the energy lost due to heat transport called the *heat current*. The heat current Q is defined as the net heat energy per second leaving the hot lead of the device due to electron transport. We hence neglect all other contributions to Q, such as phonon transport.

Each electron that contributes to the electrical current will carry some amount of heat energy equal to the difference between the electron energy and the Fermi energy in the hot lead. This energy transport summed over all electrons that contributes to the electrical current gives the total heat current, and is calculated using

$$Q = \frac{2}{h}\int_{E_{c_c}}^{\infty}(f(E,\mu_h) - f(E,\mu_c))T(E)(E-\mu_h)dE.$$

The only difference when calculating the heat current compared to electrical current is that we divide the result by e and let $(E-\mu_h)$ be part of the integral, in order to get a current of energy instead of charge.

Now when we have the power output P of the device as well as the energy loss per second Q due to heat transport, we can calculate the efficiency η by simply dividing the two:

$$\eta = \frac{P}{Q}.$$

2.8.1 The Carnot limit

There is a theoretical maximum limit to the efficiency when extracting energy using a temperature difference, called the *Carnot limit*, that is

$$\eta_C = 1 - \frac{T_c}{T_h}. \tag{2.5}$$

We will compare our calculated efficiencies to this maximum limit to get a better measure of how efficient the device really is.

Chapter 3

Results & Discussion

3.1 Interdependence between potential structure and transmission function

We now want to investigate what the transmission function looks like for different potential structures. We will calculate the transmission function for QD and superlattice structures while varying one parameter at the time, in order so see just how the transmission function depends on the different potential structure parameters.

3.1.1 Transmission function of basic structures

We begin by calculating the transmission function for different types of basic structures.

3.1.1.1 Potential step

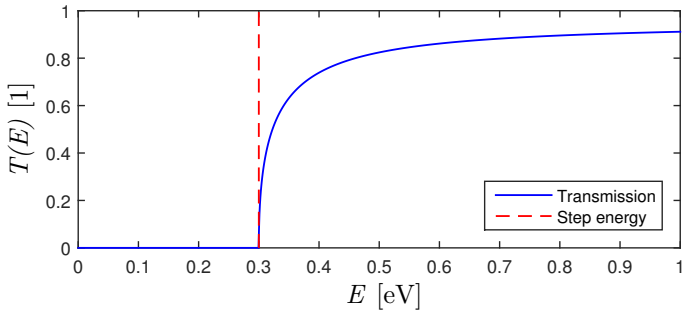

Step parameters

Height (meV)	300

FIGURE 3.1.1: Transmission function of a 300 meV high potential step.

Seen in Fig. 3.1.1 is the transmission function of a potential step. All electrons that have an energy lower than that of the step are reflected back by the structure. Electrons

with an energy higher than the step have a chance to be transmitted. The probability of transmission increases with energy.

3.1.1.2 Potential barrier

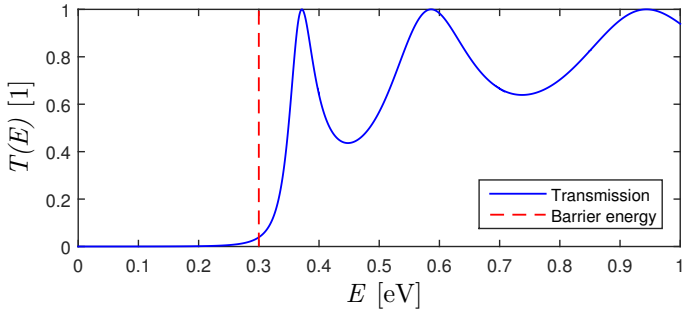

Barrier parameters

Height (meV)	300
Width (nm)	10

FIGURE 3.1.2: Transmission function of a 300 meV high and 10 nm wide potential barrier.

Seen in Fig. 3.1.2 is the transmission function of a single potential barrier. The important thing to notice is that a chance exists for an electron to be transmitted through the structure even though its energy is lower than that of the barrier. This effect is known as *tunnelling* and plays a crucial part in nanoelectronics. At energies above the barrier height the transmission function oscillates, due to resonance between the two steps in the barrier.

3.1.1.3 Double barrier (QD)

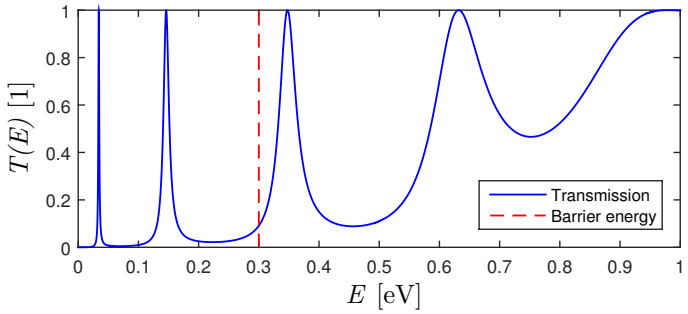

Barrier parameters

Height (meV)	300
Width (nm)	3
Distance (nm)	15

FIGURE 3.1.3: Transmission function of an 15 nm wide QD with barriers 300 meV high and 3 nm wide.

Seen in Fig. 3.1.3 is the transmission function in a double barrier QD, consisting of two barriers 3 nm wide and 300 meV high that are separated by 15 nm. The important feature of a QD that we will make use of in this project is the fact that, for symmetric barriers, the transmission probability reaches unity for discrete energies below the barrier height, due to resonances between the barriers. This extraordinary result is why QDs

can be used as very effective energy filters to control the energy of electrons that can be transmitted through he device.

3.1.1.4 Superlattice

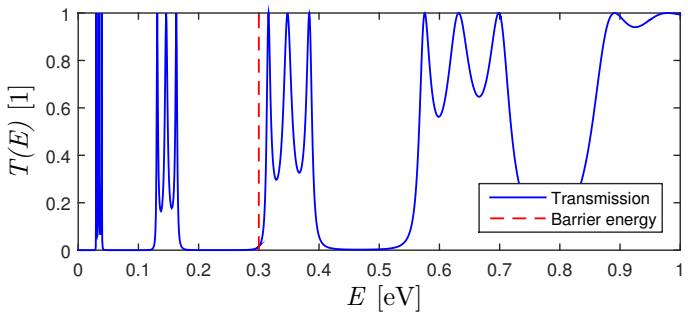

Barrier parameters

Height (meV)	300
Width (nm)	3
Distance (nm)	15
Barrier count	4

FIGURE 3.1.4: Transmission function of three 15 nm wide QDs with barriers 300 meV high and 3 nm wide.

Seen in Fig. 3.1.4 is the transmission function of a 4 barrier structure. This can be seen as a 3 QD superlattice. If we compare this graph to Fig. 3.1.3, which have barriers of the same height and dimensions, we see that each transmission peak splits up into several different peaks close to each other.

3.1.2 Influence of structure parameters on the transmission function of a QD

If we change the parameters of the potential structure, such as the height or width of the barriers, this will also change the properties of the transmission function.

We will now study how the transmission function of a QD depends on different parameters of the potential structure. Note that the scale for the transmission probability in this section is logarithmic.

3.1.2.1 Barrier height

Fig. 3.1.5 shows transmission functions for single QDs with varying barrier heights. We see that increasing the barrier height leads to a shift in the position of the transmission peak, as well as a narrowing of the peak. This narrowing of the peak makes sense since we increase the size of the obstacle the electron has to tunnel through when we increase the barrier height. The shift in peak position is a result of changing the resonances of the structure when changing the barrier height.

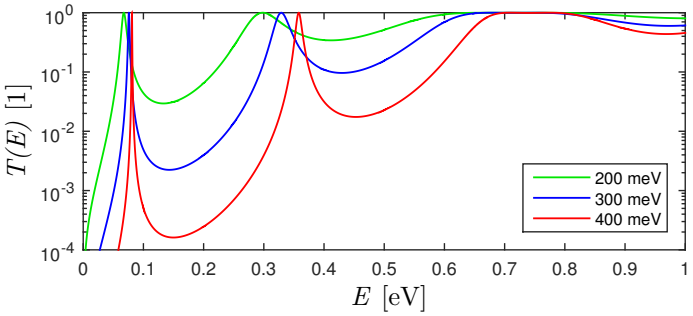

Barrier parameters

Height (meV)	(see graph)
Width (nm)	4
Distance (nm)	8
Barrier count	2

FIGURE 3.1.5: Transmission function of QDs with different barrier heights.

3.1.2.2 Barrier width

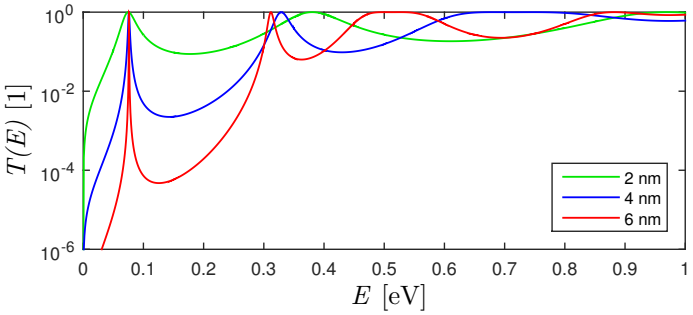

Barrier parameters

Height (meV)	300
Width (nm)	(see graph)
Distance (nm)	8
Barrier count	2

FIGURE 3.1.6: Transmission function of QDs with different barrier widths.

Fig. 3.1.6 shows transmission functions for QDs with varying barrier widths. We see that below the barrier energy, increasing the barrier width leads to a narrowing of the peaks. Above the barrier energy increasing the barrier width leads to a visible shift in the position of the transmission peak. This narrowing of the peak makes sense since we increase the length the electron has to tunnel through the barrier when we increase the barrier width. The shift in peak position is a result of changing the resonances of the structure.

3.1.2.3 Distance between barriers

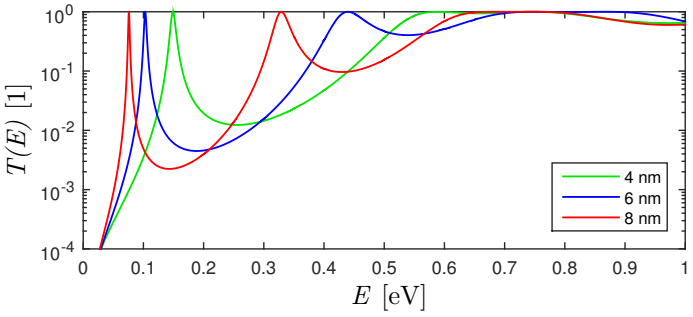

Barrier parameters

Height (meV)	300
Width (nm)	4
Distance (nm)	(see graph)
Barrier count	2

FIGURE 3.1.7: Transmission function of QDs with different distance between the barriers.

Fig. 3.1.7 shows transmission functions for QDs with varying distance between the barriers. We see that increasing the distance between the barriers leads to a shift in the position of the transmission peaks, both below and above the barrier energy. This makes sense because changing the distance between the barriers leads to a change in resonance inside the QD. At larger distances between the barriers, the transmission peaks move close to each other.

3.1.2.4 Number of barriers

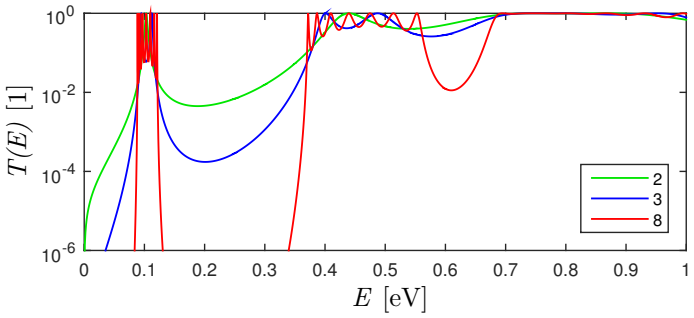

Barrier parameters

Height (meV)	300
Width (nm)	4
Distance (nm)	6
Barrier count	(see graph)

FIGURE 3.1.8: Transmission functions of structures with different number of QDs connected in series.

Fig. 3.1.8 shows transmission functions for varying number of QDs connected in series, while keeping all other parameters constant. As shown before, an increase in the number of QDs connected in series leads to a splitting of the transmission peaks. Additional QDs leads to even further splitting, and the number of transmission peaks is always equal to the number of QDs in the structure.

When adding more and more QDs into the superlattice, we see the appearance of something that looks like energy bands. Furthermore, when introducing more QDs into the structure, we also make the edges on either side of the occurring energy bands steeper. We will make great use of both of these features, as it allows us to produce a very well defined energy window in which electrons can travel.

3.1.3 Influence of structure parameters on the transmission function of a superlattice

In Sec. 3.1.2.4 we saw that adding QDs in series to form a superlattice gives rise to energy bands in the transmission function. Electrons that have an energy inside such a band have a much larger probability to be transmitted through the structure than electrons with an energy outside the band. Important to keep in mind is that the transmission probability, depending on the obstacle, can still oscillate greatly inside the energy band.

We will now investigate how the different parameters of the superlattice influence the properties of these bands. Note that, just like in the previous section, the scale for the transmission probability is logarithmic.

3.1.3.1 Barrier height

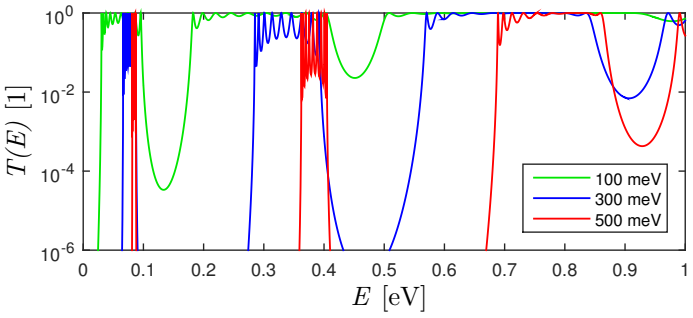

Barrier parameters

Height (meV)	(see graph)
Width (nm)	4
Distance (nm)	8
Barrier count	10

FIGURE 3.1.9: Transmission functions of superlattices with different barriers heights.

Fig. 3.1.9 shows transmission functions for superlattices with varying barrier heights. We see that increasing the barrier height gives a higher filtration of electron energies, shown in a diminishing band width as well as sharper peaks. This gives us a possibility to engineer a more well defined energy window in which electrons can flow. But it also reduces the number of electrons that can flow in the window, as sharper and more oscillating energy peaks reduce the area under the transmission function used when calculating the current as shown in Eq. (2.3). From the graph it is also clear that the bands move to higher energies when increasing the barrier height.

Important to notice is that the transmission probability stays close to unity in a larger energy interval for transmission bands above the barrier energy.

3.1.3.2 Barrier width

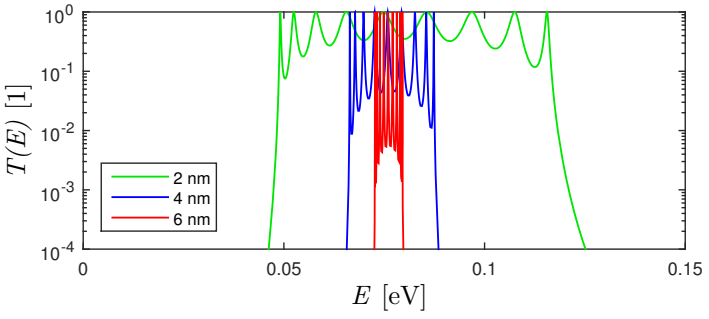

Barrier parameters

Height (meV)	300
Width (nm)	(see graph)
Distance (nm)	8
Barrier count	10

FIGURE 3.1.10: Transmission functions of superlattices with different barriers widths.

Fig. 3.1.10 shows transmission bands below the barrier energy for superlattices with varying barrier widths. We see that wider barriers gives rise to diminishing band width as well as sharper peaks, while the band positions remain unchanged.

Note that, for such thin barriers, we only need to make a tiny adjustment to the width in order to yield a great difference in the transmission function.

3.1.3.3 Distance between barriers

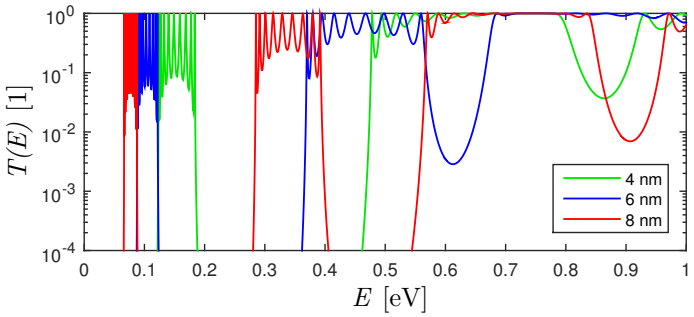

Barrier parameters

Height (meV)	300
Width (nm)	4
Distance (nm)	(see graph)
Barrier count	10

FIGURE 3.1.11: Transmission functions of superlattices with different distance between the barriers.

Fig. 3.1.11 shows transmission functions for superlattices with different distance between the barriers. We see that the bands shifts to higher energies as the distance between the barriers decrease. This is expected, as the same thing happens for the transmission peaks of a single QD as shown in Fig. 3.1.7.

The widening of the bands at higher energies is due to the electron energies being closer to the barrier height, and not an effect of changing the barrier distance parameter. Hence changing the distance between the barriers seems to be an effective way of shifting the positioning of the energy bands to different energies, without changing anything else about the transmission function.

3.1.3.4 Number of barriers

Fig. 3.1.12 shows transmission bands for superlattices with different number of barriers in the structure. We see that as we add more barriers into the structure, the band width increases up to a certain point. The bands also become more well defined, without becoming more unstable (unstable meaning the transmission function oscillating down to lower values) inside the band, as it did when changing the height and width of the barriers as seen in Fig. 3.1.9 and 3.1.10.

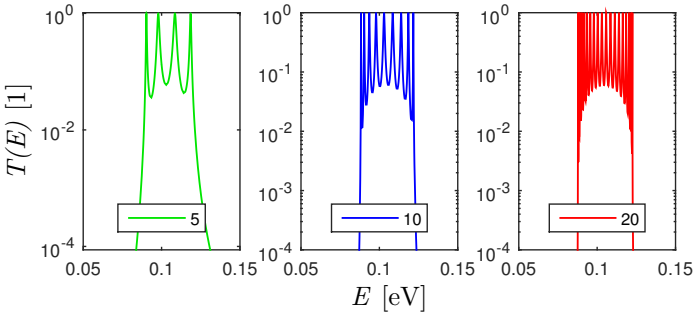

Barrier parameters

Height (meV)	300
Width (nm)	4
Distance (nm)	6
Barrier count	(see graph)

FIGURE 3.1.12: Transmission functions of superlattices with different number of barriers.

3.2 Optimizing the transmission function

As mentioned in Sec. 1.5 one of the main things to focus on is to engineer a transmission function with a rectangular shape, as shown in Fig. 3.2.1, and to try to accomplish this using a NW embedded with a QD superlattice.

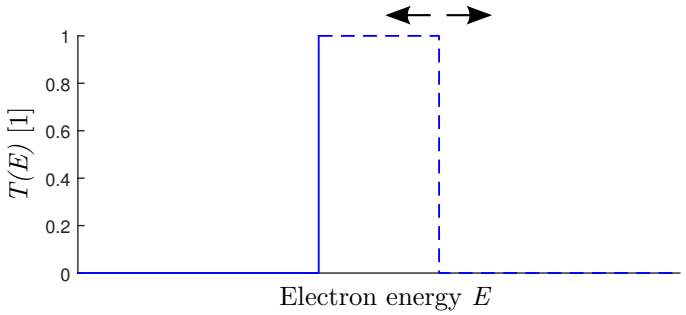

FIGURE 3.2.1: Optimal rectangular transmission function with variable width.

The low-energy side of the rectangular transmission function should as mentioned in Sec. 1.4 be positioned above the Fermi level, in order to prohibit electron transport from the cold to the hot lead. However, this feature has not only to do with the transmission function, but is accomplished by doping and/or gating the leads in order to put the Fermi level at the desired energy.

In order to maximize the power output, the rectangular transmission function should have an infinite width. That way, all electrons above the Fermi energy contribute to the current. However, as mentioned in Sec. 1.2, this also means much of the current is carried through high energy electrons, additionally leading to a high heat current and hence a diminishing efficiency.

From an efficiency point of view, the optimal transmission function is rectangular with an infinitesimal width positioned above the Fermi energy [15]. In this case, all electrons that are part of the transport will carry close to no heat current. An obvious drawback to

this is that, because the electrical current depends on the integral under the transmission function, the power output from such a device would be negligible.

The best thing would be to have a way to engineer a relatively wide rectangular transmission function, with the possibility to make it narrower if a higher efficiency is desired.

In Fig. 2.5 it is clear that a transmission band with a width of approximately 4 meV in the cold and 150 meV in the hot temperature regime is sufficient to enable transmission of a majority of the electrons above the Fermi level, and hence maximize the power output. These widths could then be made narrower in order to increase the efficiency, at the cost of a decreased power output.

But more important than lining up the transmission band with the positive parts in Fig. 2.5, is to make sure the negative parts are not inside the next transmission band below it in energy, since that would lead to electron transport in the wrong direction. From Fig. 2.5 we see that the widths of the negative parts are approximately 8 meV and 250 meV in the cold and hot regime respectively, so this should also be the minimum allowed distance to the transmission band below the one we choose for transmission.

By utilizing what was shown in the precious section, about how we are able to modify the transmission function by changing the structure parameters, we will now construct two different types of transmission functions.

We want both types to have rectangular shapes, but one type we want to contain a wide transmission band in order to maximize the output power, and the other type we want to have a very narrow transmission band in order to maximize the efficiency.

Work flow When obtaining the transmission functions in the following sections, the knowledge gained from the previous sections on how different parameters affect the transmission function was utilized along a trial and error process, in order to retrieve the desired transmission functions. The output power and efficiency of these transmission functions was calculated, and optimized by tweaking the potential structure parameters and recalculating the transmission functions.

3.2.1 Transmission above the barriers for maximum power output

In order to get a large current, it is necessary for the transmission function to remain close to unity in a larger interval. The only time this seems to happen is when the transmission band lies above the barrier height, as can be seen in Fig. 3.1.9.

We will in the following paragraphs try to accomplish transmission functions with a rectangular transmission band above the barrier height suitable both for the cold and hot temperature regime.

3.2.1.1 Cold temperature regime

By using appropriate parameters for the potential structure, we generate the transmission function shown in Fig. 3.2.2A.

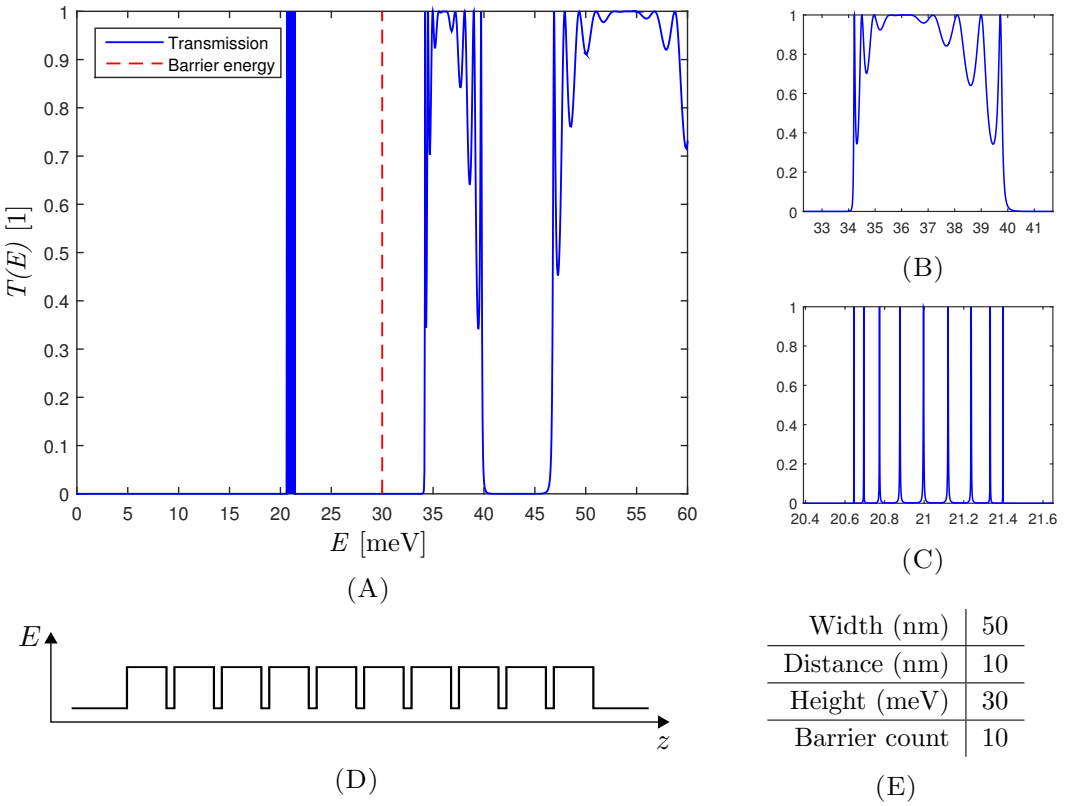

FIGURE 3.2.2: (A) The transmission function for transport above the barrier height in the cold temperature regime. (B) The magnified transmission band used for transport. (C) The magnified transmission peaks below the transmission band. (D) The potential structure the transmission function is calculated from. (E) The structure dimensions.

Fig. 3.2.2B shows a magnification of the second lowest transmission band: the one that will be used for electron transport. The shape of the band is much like that of a rectangle, and it is wide enough to enable transport of all electrons from the hot to the cold lead, as mentioned in the introduction to Sec. 3.2, hence the power output will be maximized.

The distance between the transmission band and the band below it is also sufficiently large to prevent a back flow of electrons from the cold to the hot lead. Even if these

bands would have been closer to each other, the back flow would still be very small since the lowest transmission band in the transmission function is very peaked and hence has a very small area under it, as can be seen in Fig. 3.2.2C.

The potential structure used to calculate the transmission function is shown in Fig. 3.2.2D and the barrier dimensions are given in Tbl. 3.2.2E.

This superlattice does not work as in conventional applications, where the desired transmission band is at an energy below the barrier energy. In this case, we make use of the resonances in the superlattice in another way. Instead of splitting a transmission peak below the barrier energy, that is made possible by tunnelling, we deliberately diminish all transmission below the barrier energy by making the barriers very thick, in order to prohibit back flow of electrons. The resonances in the structures reflect certain energies above the barriers, up until the transmission band begins. Inside the transmission band, constructive interference results in the transmission retaining a high value throughout the band.

This is an innovative way to engineer a rectangular transmission function, but it is very difficult to make the transmission band narrow, which is needed to increase the efficiency. But if a maximum power output is desired, this approach seems promising.

3.2.1.2 Hot temperature regime

We generate a transmission function adapted to give a high power output in the hot temperature regime, shown in 3.2.3A.

Compared to the transmission function in the cold regime there are a few differences, even though they look very similar.

Most importantly the physical dimensions of the structure need be decreased as can be seen in Tbl. 3.2.3E, in order to form wide and well defined transmission bands on a larger energy scale. The barrier height must in turn be increased in order to place the transmission band between the two lowest bands in the transmission function.

As can be seen in Fig. 3.2.3B, the transmission band is not wide enough to allow transmission for all electrons above the Fermi level. This would require the structural dimensions to be decreased even further, which would be a difficult structure to realize in practice. The result of this is that the power output will not be truly maximized, but close to it.

For the same reason, the energy gap between the two lowest bands is not sufficient to completely block the back flow of electrons. The back flow is suppressed by the fact that

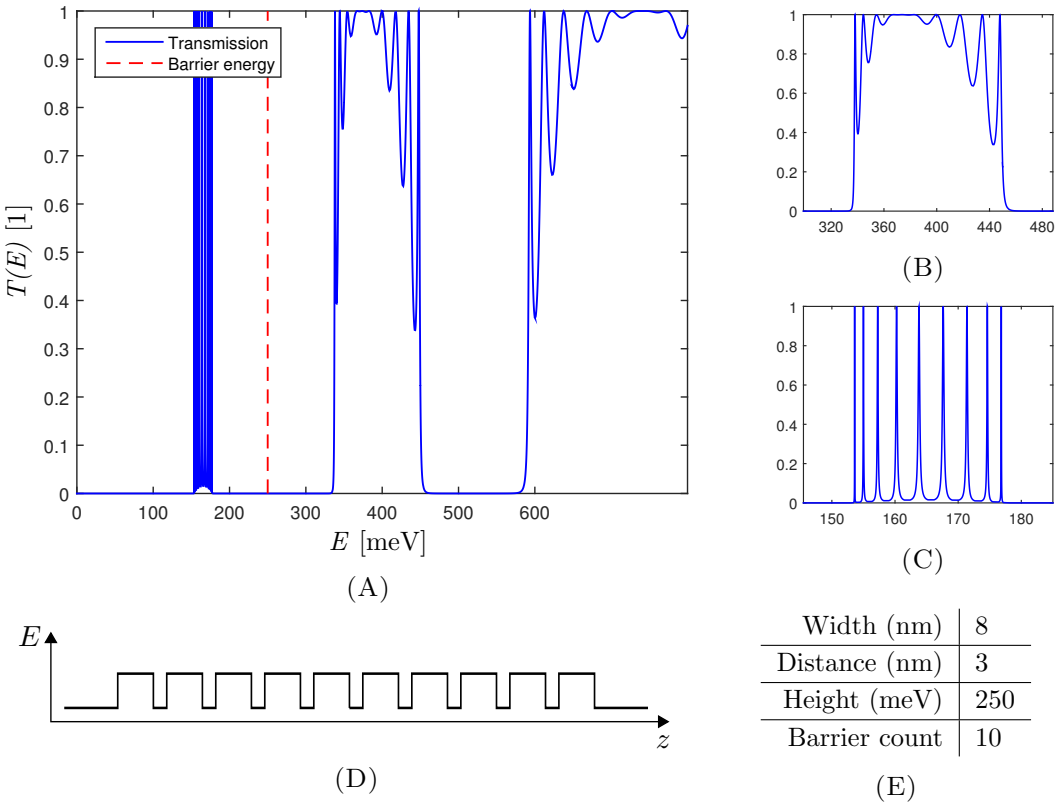

Width (nm)	8
Distance (nm)	3
Height (meV)	250
Barrier count	10

FIGURE 3.2.3: (A) The transmission function for transport above the barrier height in the hot temperature regime. (B) The magnified transmission band used for transport. (C) The magnified transmission peaks below the transmission band. (D) The potential structure the transmission function is calculated from. (E) The structure dimensions.

the lowest transmission band is very peaked, as can be seen in Fig. 3.2.3C. This band will still decrease the efficiency though, as it will carry very low energy electrons to the hot lead, being so far from the Fermi level.

3.2.2 Maximize the efficiency with antireflection coating

A way of making the transmission function smoother is to put so called antireflection coating on either side of the obstacle [16]. This is in practice done by making the barriers to the outermost left and right of the superlattice half the width compared to the rest of the barriers.

Utilizing this technique it is possible to give the first transmission band, at a position below the barrier energy, a rectangular shape. Because it is the first transmission band in the transmission function, it is easy to modify its width using techniques described in Sec. 3.1.3, without having to worry about another transmission band at a lower energy allowing transport in the wrong direction.

We will now show that by using antireflection coating it is possible to obtain very narrow transmission bands, both in the cold and hot temperature regime, in order to maximize the efficiency. As mentioned before, this will lead to a very small power output. But contrary to the transmission functions in Sec. 3.2.1 where it was difficult to decrease the band width in order to increase the efficiency, it is in this case easy to broaden the bands in order to increase the power output. This is done using techniques described in Sec. 3.1.3 by either decreasing the barrier height or width.

3.2.2.1 Cold temperature regime

Shown in Fig. 3.2.4A is the transmission function and Fig. 3.2.4B shows the magnified transmission band used for transport. The transmission function is calculated from the potential structure shown in Fig. 3.2.4C and its dimensions can be seen in Tbl. 3.2.4D.

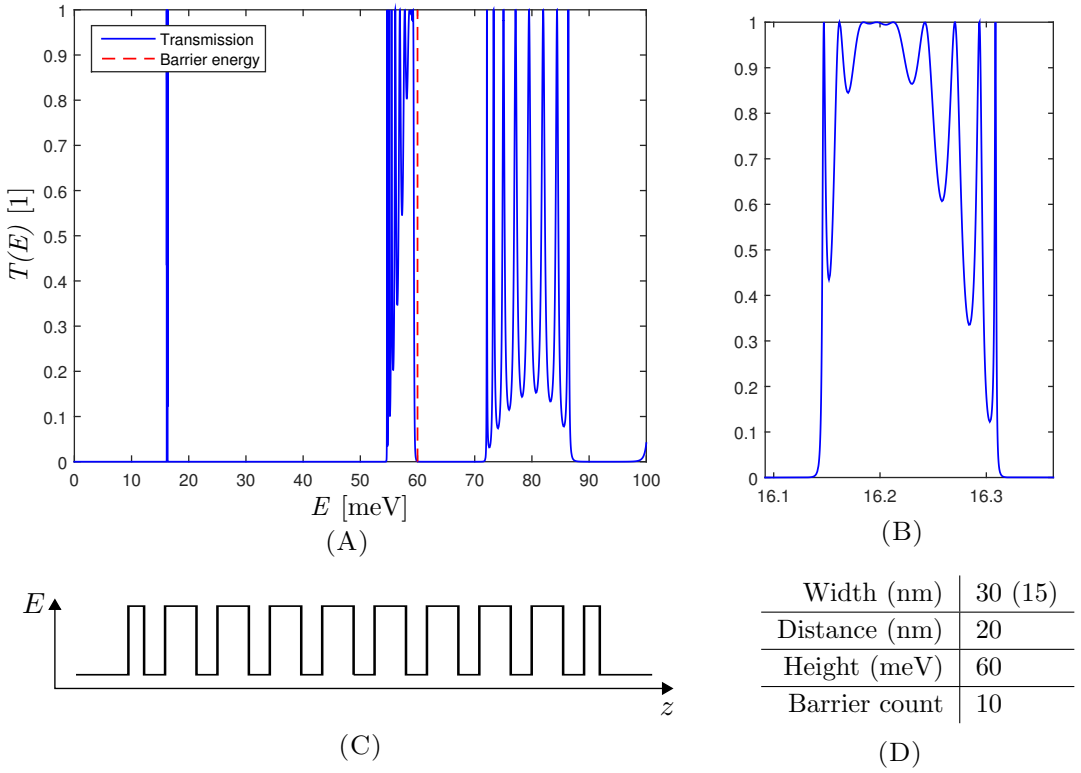

Width (nm)	30 (15)
Distance (nm)	20
Height (meV)	60
Barrier count	10

FIGURE 3.2.4: (A) The transmission function when using antireflection coating in the cold regime. (B) The magnified transmission band used for transport. (C) The potential structure the transmission function is calculated from. (D) The structure dimensions.

We see that the transmission band below the barrier energy, that in previous calculations became very peaked as shown in Fig. 3.2.2C and 3.2.3C, obtain a rectangular shape

when using antireflection coating. The width of the band is very small, which should yield a high efficiency, at the cost of a greatly reduced output power. But the power output can as mentioned before quite easily be increased by decreasing either the barrier height or width, which would also decrease the efficiency.

3.2.2.2 Hot temperature regime

Shown in Fig. 3.2.5A is the transmission function and Fig. 3.2.5B shows the magnified transmission band used for transport. The transmission function is calculated from the potential structure shown in Fig. 3.2.5C and its dimensions can be seen in Tbl. 3.2.5D.

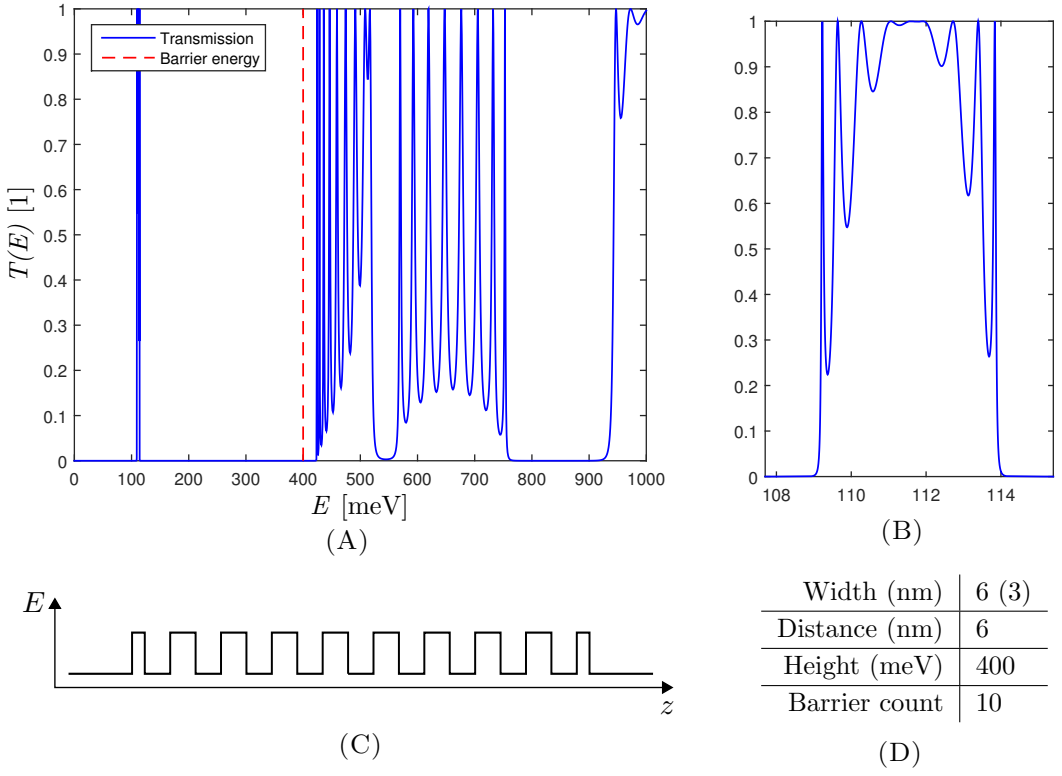

Width (nm)	6 (3)
Distance (nm)	6
Height (meV)	400
Barrier count	10

FIGURE 3.2.5: (A) The transmission function when using antireflection coating in the hot regime. (B) The magnified transmission band used for transport. (C) The potential structure the transmission function is calculated from (D) The structure dimensions.

Similarly to Sec. 3.1.3, smaller barrier dimensions are required in the hot temperature regime.

The reason for the width having to be small is to ensure the transmission band has some width whatsoever.

The distance between the barriers is required to be small in order to be able to match the transmission band to the positive peak in the Fermi distributions subtracted from each other, as shown in Fig. 2.5A. An alternative to this would be to put the Fermi energy inside the band gap by less heavy doping.

3.3 Power and efficiency

Now that we have done a thorough investigation of how to optimize the transmission function, it is time to calculate what power output and efficiency we get from the devices engineered in Sec. 3.2.1 and 3.2.2.

We want to compare the results obtained from those transmission functions, to those obtained from a single QD. The transmission function of a QD can be approximated to a Lorentzian distribution, like the one in Fig. 3.3.1.

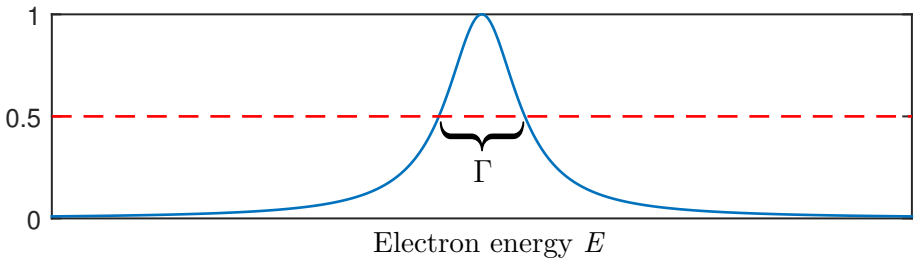

FIGURE 3.3.1: A Lorentzian distribution with width Γ.

Both the output power and efficiency will depend on the position of the Fermi levels in the leads as well as the bias voltage over the structure. We will perform the comparison at a point where the output power is at its maximum, in order to have some consistency in our comparisons. The width of the Lorentzian will be set so that the efficiency at maximum output power calculated using the Lorentzian as the transmission function is the same as the efficiency at maximum output power calculated from our optimized transmission function. We will then compare the maximum output power obtained when using the Lorentzian to the maximum output power when using the optimized transmission function, to see if there is any improvement.

3.3.1 Transport above the barrier energy

We begin by calculating the output power and efficiency for transport above the barriers, using the transmission function calculated in Sec. 3.2.1.

3.3.1.1 Cold temperature regime

The output power and efficiency for transport above the barrier energy in the cold temperature regime calculated using the transmission function in Fig. 3.2.2A is shown in Fig. 3.3.2.

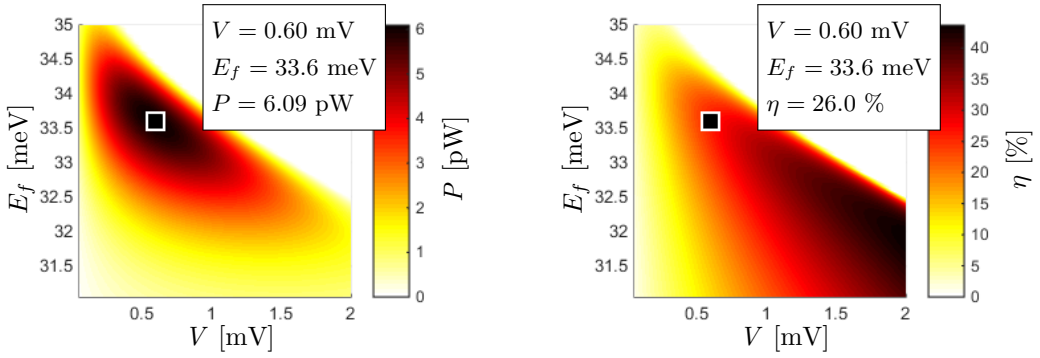

(A) Output power. (B) Efficiency.

FIGURE 3.3.2: (A) Output power and (B) efficiency, using the transmission function for transport above the barrier energy in the cold regime, as shown in Fig. 3.2.2A.

If we compare the graphs to the transmission function in Fig. 3.2.2A, we see that maximum output power is achieved by placing the Fermi level slightly below the transmission band, as expected. The highlighted reference point shows the point of maximum output power.

If we compare the calculated efficiency at maximum output power with the maximum theoretical Carnot efficiency that for these temperatures is 60%, see Eq. (2.5), we see that $\eta = 0.43\eta_C$. This can be increased however, by increasing the bias voltage and lowering the average Fermi level in the leads, to the cost of a reduced output power.

To compare the maximum output power to that of a single QD with the same efficiency at maximum output power, we perform the same calculations using a Lorentzian distribution as the transmission function. The results can be seen in Fig. 3.3.3.

We see that, at the reference points chosen, the output power using the optimized transmission function yields an output power 4.1 times higher than when using a Lorentzian distribution as the transmission function.

3.3.1.2 Hot temperature regime

The output power and efficiency for transport above the barrier energy in the hot temperature regime calculated using the transmission function in Fig. 3.2.3A is shown in Fig. 3.3.4.

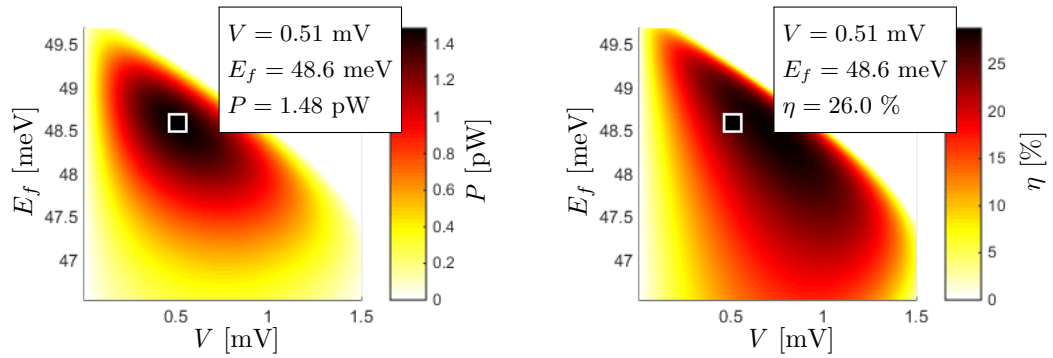

(A) Output power. (B) Efficiency.

FIGURE 3.3.3: (A) Output power and (B) efficiency in the cold regime, using a Lorentzian distribution centred at 50 meV as the transmission function.

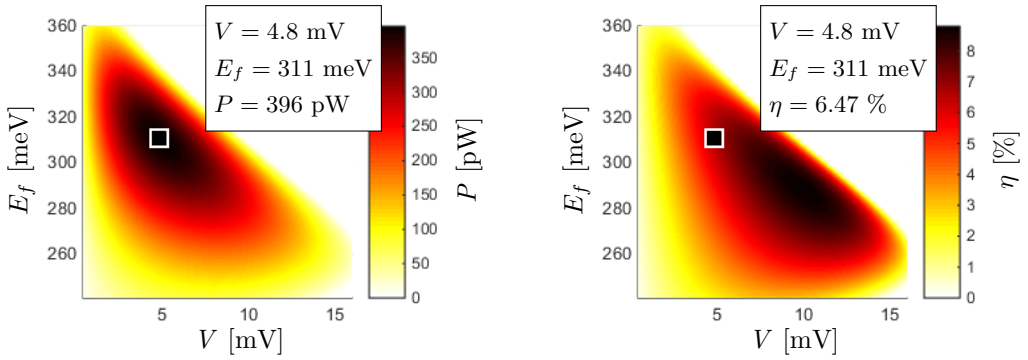

(A) Output power. (B) Efficiency.

FIGURE 3.3.4: (A) Output power and (B) efficiency, using the transmission function for transport above the barrier energy in the hot regime, as shown in Fig. 3.2.3A.

Compared to the cold temperature regime, the output power in the hot temperature regime is much higher. This is because there is a larger temperature difference between the leads.

The Carnot efficiency is in this temperature regime 16.7%, which means that $\eta = 0.39\eta_C$.

Output power and efficiency using a Lorentzian distribution with a width set to yield the same efficiency at maximum output power can be seen in Fig. 3.3.5.

We see that by using the optimized transmission function the output power improves by a factor of 4.5.

3.3.2 Using antireflection coating

We will now calculate the output power and efficiency for the transmission functions calculated in Sec. 3.2.2, where a structure with antireflection coating was used to calculate the transmission function.

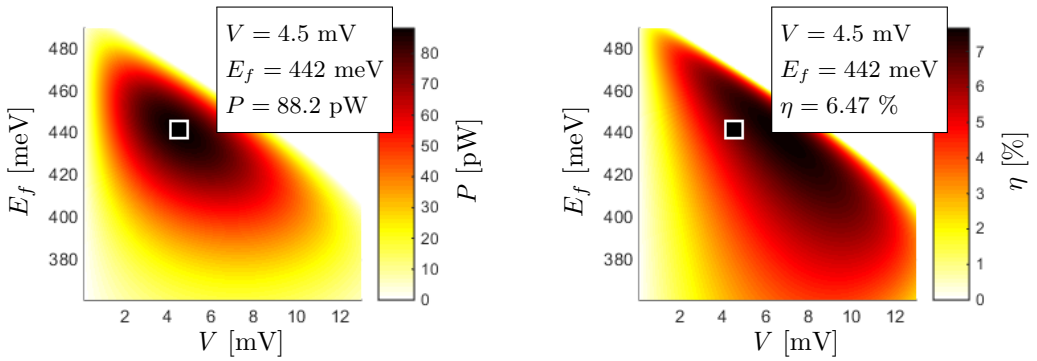

(A) Output power. (B) Efficiency.

FIGURE 3.3.5: (A) Output power and (B) efficiency in the hot regime, using a Lorentzian distribution centred at 500 meV as the transmission function.

3.3.2.1 Cold temperature regime

Output power and efficiency calculated using the transmission function in Fig. 3.2.4A is shown in Fig. 3.3.6.

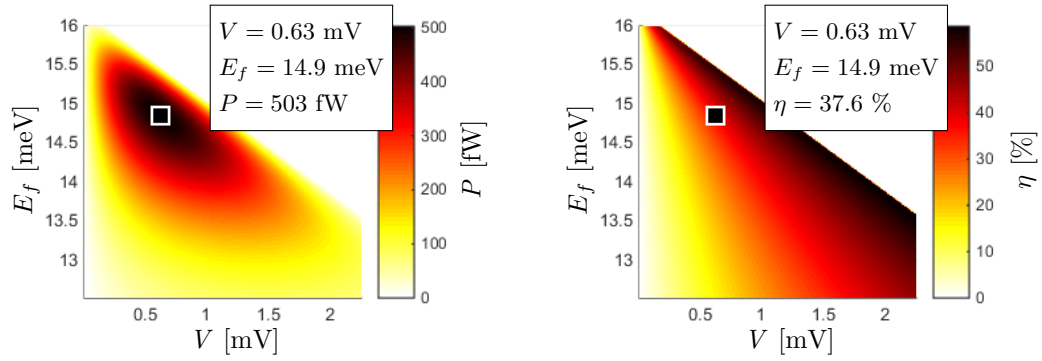

(A) Output power. (B) Efficiency.

FIGURE 3.3.6: (A) Output power and (B) efficiency, using the transmission function calculated from a barrier structure with antireflection coating in the cold regime, as shown in Fig. 3.2.4A.

It is clear that this type of structure yields a much higher efficiency, and it is theoretically possible to come very close to the Carnot limit at 60%. At maximum output power, the efficiency $\eta = 0.63\eta_C$. But as mentioned before, this improvement comes at the cost of a much decreased output power, due to the very narrow transmission band.

It will now be very interesting to compare this result to the output power we get from a simulated QD with the same efficiency, shown in Fig. 3.3.7.

An improvement in the output power by a factor of 41.6 can be seen when using the optimized transmission function with antireflection coating. The reason for this great improvement is that the Lorentzian shape of the transmission peak of a QD is intrinsically bad if a high efficiency is desired. This is because there will always be a tail leading

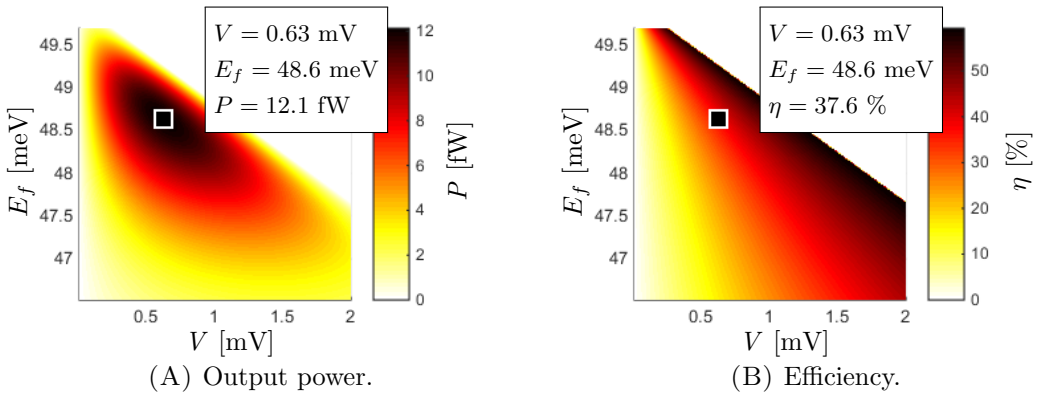

(A) Output power. (B) Efficiency.

FIGURE 3.3.7: (A) Output power and (B) efficiency in the cold regime, using a Lorentzian distribution centred at 50 meV as the transmission function.

up to the peak that will allow transport of electrons in the wrong direction, as can be seen in Fig. 3.3.1. This means that the Lorentzian has to be made very narrow in order to reach a high efficiency, which will in turn decrease the output power.

3.3.2.2 Hot temperature regime

Output power and efficiency calculated using the transmission function in Fig. 3.2.5A is shown in Fig. 3.3.8.

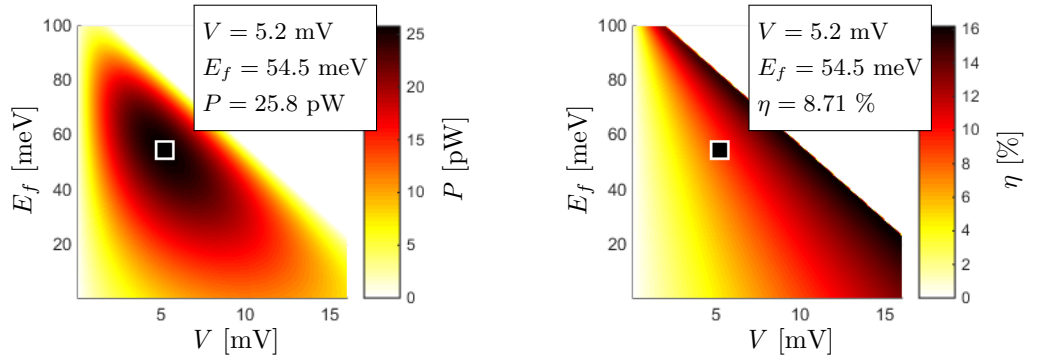

(A) Output power. (B) Efficiency.

FIGURE 3.3.8: (A) Output power and (B) efficiency, using the transmission function calculated from a barrier structure with antireflection coating in the hot regime, as shown in Fig. 3.2.5A.

As in the cold regime, it is possible to come very close to the Carnot efficiency which is 16.7%, to the cost of a reduced output power.

We can compare this result to when using a Lorentzian as the transmission function, shown in Fig. 3.3.9.

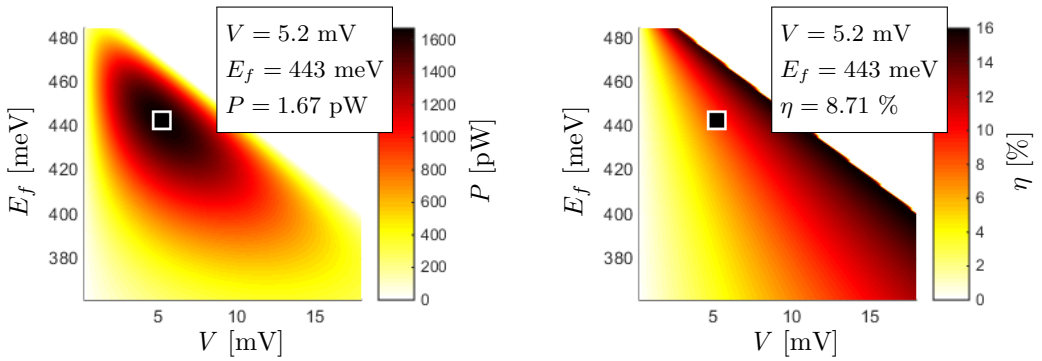

(A) Output power. (B) Efficiency.

FIGURE 3.3.9: (A) Output power and (B) efficiency in the hot regime, using a Lorentzian distribution centred at 500 meV as the transmission function.

Here we see an increase by a factor of 15.5 in the maximum output power, for the same reasons mentioned previously. This factor would probably increase even further if the transmission band in the optimized transmission function was made even narrower.

3.4 Output power and efficiency dependence on the number of barriers

The previous section verifies that it is possible to increase the output power without decreasing the efficiency, by using a QD superlattice instead of a single QD. In all calculations when calculating the output power and efficiency in Sec. 3.3, 10 barriers were used when calculating the transmission function.

We will now investigate how the maximum output power and the efficiency at maximum output power depends on the number of barriers in the potential structure. This will be done by modifying the structures used in Sec. 3.2.1 and 3.2.2 to consist of different number of barriers, and use these potential structures to calculate their respective transmission function. The maximum output power and the efficiency at maximum output power will then be calculated using these transmission functions, and the results plotted against the number of barriers used in each respective structure.

3.4.1 Transport above the barrier energy

Initially we consider the structures used in Sec. 3.2.1, where the transmission band used for transport lies above the barrier height, in order to maximize the output power.

3.4.1.1 Cold temperature regime

The maximum output power and efficiency at maximum output power as a function of the number of barriers in the potential structure can be seen in Fig. 3.4.1.

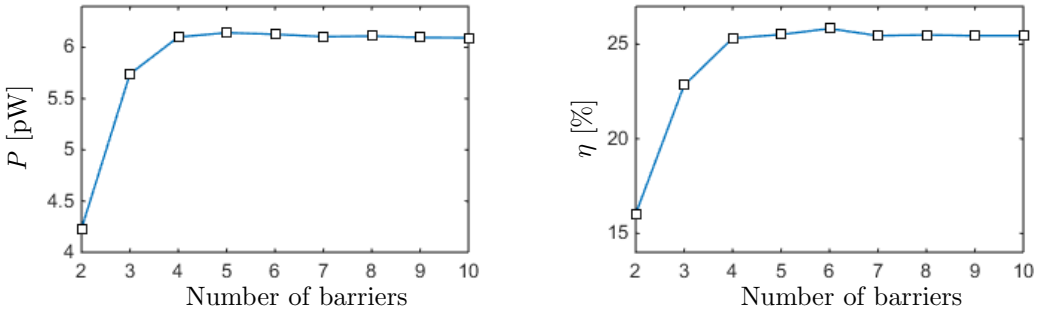

(A) Maximum output power. (B) Efficiency.

FIGURE 3.4.1: (A) Maximum power output and (B) efficiency at maximum output power when changing the number of barriers when calculating the transmission function in Fig. 3.2.2A.

We see that both the maximum output power as well as the efficiency at maximum output power increases up until 4 barriers. Increasing the size of the superlattice beyond that by adding more barriers into the structure change neither the maximum output power nor the efficiency at maximum output power.

This result can be understood when studying the rightmost transmission peaks in Fig. 3.1.8. Keep in mind that the transmission band is very wide relative to the electron distribution, so the increase in band width by increasing the number of barriers leads to a relatively small increase in output power. Much of the increase in output power when adding more barriers comes instead from making the lower transmission band edge sharper, preventing transport in the wrong direction. But already after adding a few extra barriers, this edge is is sharp enough to stop the majority of electron transport in the wrong direction, so little is gained from adding more barriers beyond that.

3.4.1.2 Hot temperature regime

The maximum output power and efficiency at maximum output power as a function of the number of barriers in the potential structure can be seen in Fig. 3.4.2.

Again, we conclude that extending the structure beyond 4 barriers does little to improve the performance in terms of output power and efficiency.

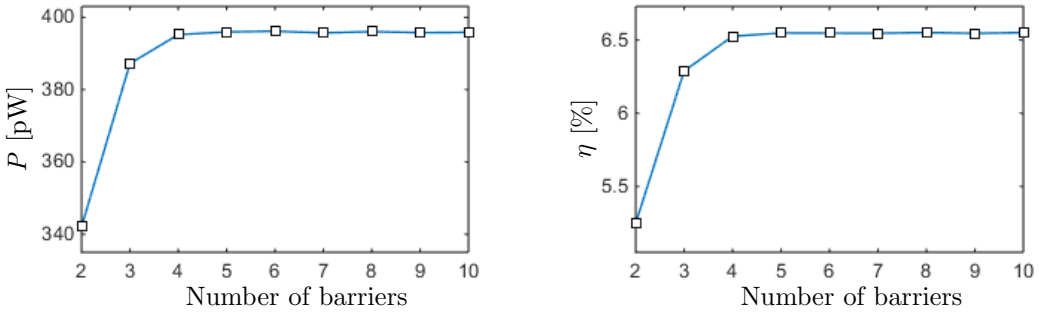

(A) Maximum output power. (B) Efficiency.

FIGURE 3.4.2: (A) Maximum power output and (B) efficiency at maximum output power when changing the number of barriers when calculating the transmission function in Fig. 3.2.3A.

3.4.2 Using antireflection coating

We do the same thing for the structures with antireflection coating calculated in Sec. 3.2.2 where we tried to maximize the efficiency.

3.4.2.1 Cold temperature regime

The maximum output power and efficiency at maximum output power as a function of the number of barriers in the potential structure can be seen in Fig. 3.4.3.

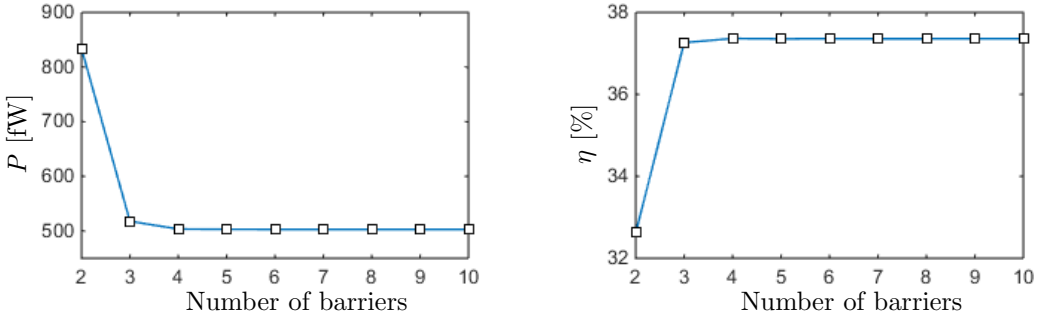

(A) Maximum output power. (B) Efficiency.

FIGURE 3.4.3: (A) Maximum power output and (B) efficiency at maximum output power when changing the number of barriers when calculating the transmission function in Fig. 3.2.4A.

At first glance the first data point for 2 barriers, representing a single QD, seems to yield quite good results, with a much higher output power and only a slightly decreased efficiency compared to the other data points. But when using antireflection coating we focus on getting a high efficiency, and if the QD in question were to be modified to have an efficiency equal to those of the rest of the data points, the maximum output power

would drop below those of the rest of the data points. This tells us that we lose a lot of output power if a very high efficiency is desired.

Because we use a structure with antireflection coating, where the two outermost barriers are thinner than the rest, the cases with 2 and 3 barriers in the structure are a bit different and not really comparable to the rest of the data points, and will hence be disregarded.

The case with 4 barriers can be seen as a single QD with added antireflection coating, and we see that there is improvement neither with respect to the output power nor the efficiency when adding more barriers. The reason is that 4 barriers are enough to make the transmission band edges sufficiently sharp, and adding more barriers does not change the overall looks of the transmission function to any large extent.

3.4.2.2 Hot temperature regime

The maximum output power and efficiency at maximum output power as a function of the number of barriers in the potential structure can be seen in Fig. 3.4.4.

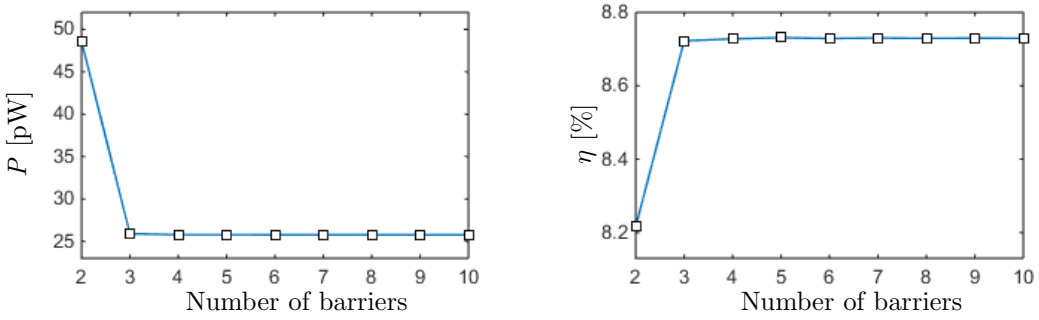

(A) Maximum output power. (B) Efficiency.

FIGURE 3.4.4: (A) Maximum power output and (B) efficiency at maximum output power when changing the number of barriers when calculating the transmission function in Fig. 3.2.5A.

The result is the same as in the cold regime, and there is nothing to be gained in terms of output power and efficiency from having more than 3 barriers in the structure.

3.5 Asymmetric barrier dimensions

In order do extract a decent amount of power from a NW based thermoelectric device in practice, it is of course necessary to use many NWs in the same element. One way to do this would be to connect many NWs in parallel, as in Fig. 3.5.1.

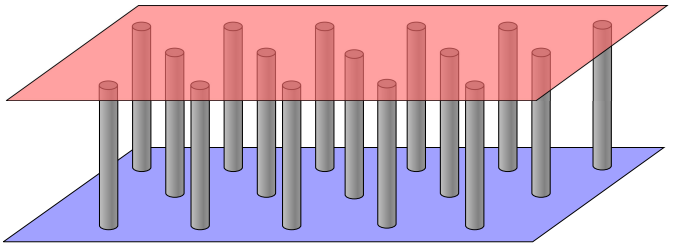

FIGURE 3.5.1: Illustration of a NW array with many NWs conneted in parallel between two heat sinks.

The total output power would then equal the output power from one NW, times the number of NWs.

But most likely, the NWs' potential structures would not be as perfect as the ones we have been modelling, but the structure dimensions such as the barrier widths and the distances between the barriers would differ from each other slightly. Since the transmission function is dependent on resonances in the potential structure, altering its dimensions to make it less symmetric could have a great impact on the transmission function.

To get a feeling for how sensitive the transmission function is to an asymmetric potential structure, we will calculate many (10 000) transmission functions with barrier widths and distances that are randomly generated from a *normal distribution* centred around the desired length. We then show the *average transmission function* $T_{av}(E)$ where the transmission probability for a certain energy is the average transmission probability for that energy from all N transmission functions:

$$T_{av}(E) = \frac{1}{N}\sum_{n=1}^{N} T_n(E). \tag{3.1}$$

We will do this for the transmission band for transport above the barriers, as previously shown in Fig. 3.2.2B and 3.2.3B. We do it both in the cold and hot temperature regime because the structure dimensions in the hot regime are much smaller than in the cold, and we want to be able to compare these two cases. We will do the calculations both using 10 barriers, because that is what we have used in most calculations, and 4 barriers, because it was in Sec. 3.4 shown that neither the maximum output power nor the efficiency improves beyond this point.

The barrier widths and distances used in the calculations for one of the cases, 4 barriers in the cold temperature regime, are shown in Fig.

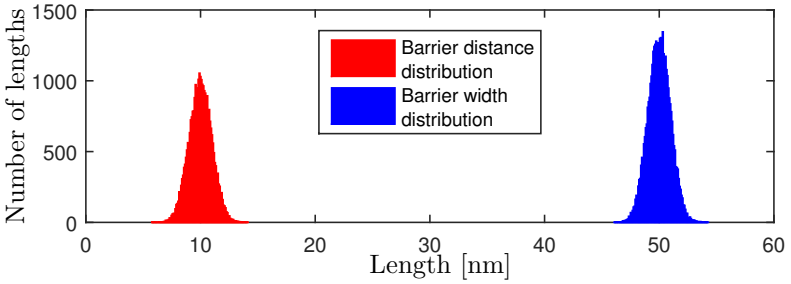

FIGURE 3.5.2: Length distributions of barrier width and distance between barriers.

The barrier widths and distances are randomly generated from normal distributions centred around 50 nm and 10 nm respectively. The standard deviation used in both cases is 1 nm.

The average transmission functions for all cases can be seen in Fig. 3.5.3.

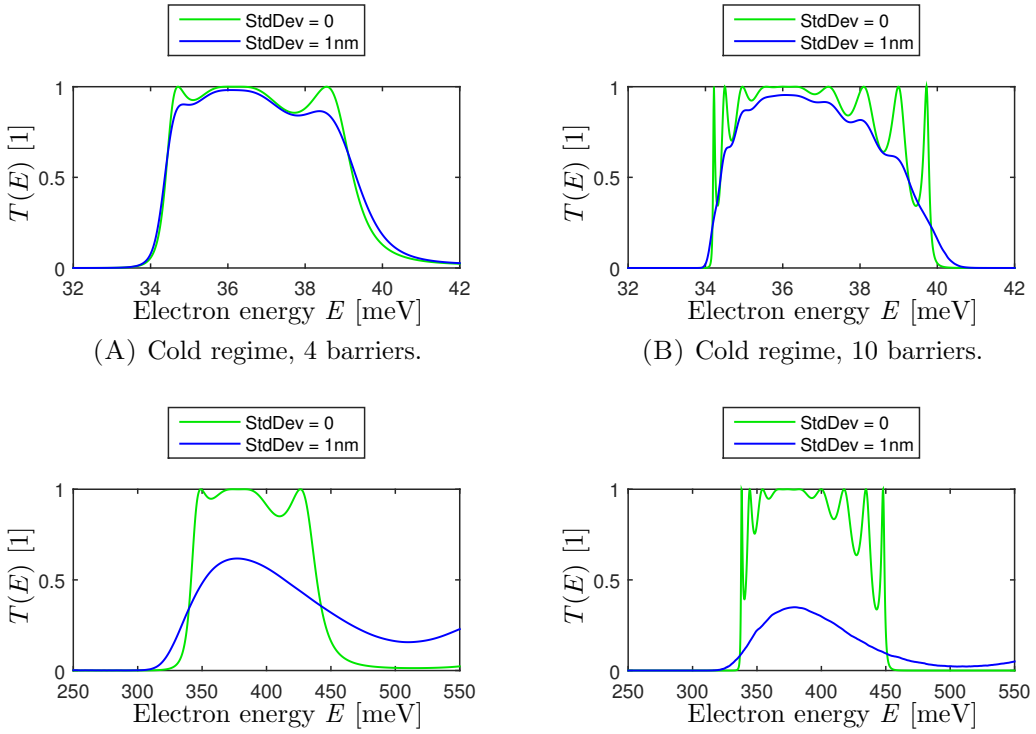

(A) Cold regime, 4 barriers.

(B) Cold regime, 10 barriers.

(C) Hot regime, 4 barriers.

(D) Hot regime, 10 barriers.

FIGURE 3.5.3: Average transmission functions of symmetric (green) and asymmetric (blue) potential structures.

We see that an asymmetric structure has a smoothing effect on the otherwise oscillating transmission band. It also lowers the transmission function, so that it no longer reaches unity.

As expected, the transmission function in the hot regime is, due to its smaller dimensions, more sensitive to an asymmetric potential structure. This can be seen when comparing Fig. 3.5.3A to Fig. 3.5.3C or Fig. 3.5.3B to Fig. 3.5.3D.

It is also clear that the transmission function becomes more sensitive to an asymmetric structure if the number of barriers is increased, as can be seen when comparing Fig. 3.5.3A to Fig. 3.5.3B or Fig. 3.5.3C to Fig. 3.5.3D.

If we want to calculate the average current for each NW in a NW array with N NWs such as the one in Fig. 3.5.1 we can use a modified version of Eq. (2.3):

$$\begin{aligned} I_{av} &= \frac{1}{N}\sum_{n=1}^{N}\frac{2e}{h}\int_{E_{c_c}}^{\infty}(f(E,\mu_c)-f(E,\mu_h))T_n(E)dE \\ &= \frac{2e}{h}\int_{E_{c_c}}^{\infty}(f(E,\mu_c)-f(E,\mu_h))\frac{1}{N}\sum_{n=1}^{N}T_n(E)dE \\ &\overset{(3.1)}{=} \frac{2e}{h}\int_{E_{c_c}}^{\infty}(f(E,\mu_c)-f(E,\mu_h))T_{av}(E)dE \\ &\overset{(2.3)}{=} I(T(E)=T_{av}(E)). \end{aligned}$$

We see that the average current is calculated using the same formula as previously, but replacing the transmission function with the average transmission function that we just calculated.

3.5.1 Impact of asymmetry on output power and efficiency

The output power and efficiency using the transmission functions in Fig. 3.5.3 has been calculated, but the plots are not shown in this report due to the results being quite intuitive. In the hot temperature regime, with relatively small barrier dimensions, both the output power and the efficiency was very much degraded. In the cold regime, with relatively large barrier dimensions, there was not much difference regarding neither the output power nor the efficiency.

To understand these results we need to remember the important features of the transmission band: having a sharp lower band edge and a large total area where the maximum transmission value reaches unity.

In the cold regime, both of these features stay true when making the barrier dimensions asymmetric. Even though the transmission function no longer follow the former peaks reaching unity, the area inside those peaks is relatively small, so the impact on the performance is also small. In the hot regime however, the lower transmission band edge

very much looses its sharpness, and the maximum transmission value also reaches far from unity leading to a smaller total area.

3.6 1D and 3D output power comparison

Finally, we will calculate the output power in the 3D case and compare it to the 1D case. In practice, this can be realized by placing very thin semiconductor sheets on top of each other and connect the top and bottom sheet to heat sinks with different temperatures [17].

As described in Sec. 2.6 we will use the current density J in the calculations, which will give the output power per unit area. In order to be able to compare the results to the 1D case, the 3D current density as well as the 3D output power density will be normalized so that the current density at maximum output power density in the 3D case equals the current at maximum output power in the 1D case. We will then compare the maximum output power in the 1D and 3D case. This normalization can seem a bit arbitrary, but will give some indication if there is anything to be gained using thermoelectric elements based on 1D structures such as NWs, instead of conventional bulk structures. We will only do this using the transmission functions for transport above the barriers, both in the cold and hot temperature regime, calculated in Sec. 3.2.1.

3.6.1 Transport above the barriers - cold temperature regime

Fig. 3.6.1 shows the output power calculated before in Sec. 3.3.1 as well as the current, for the 1D case.

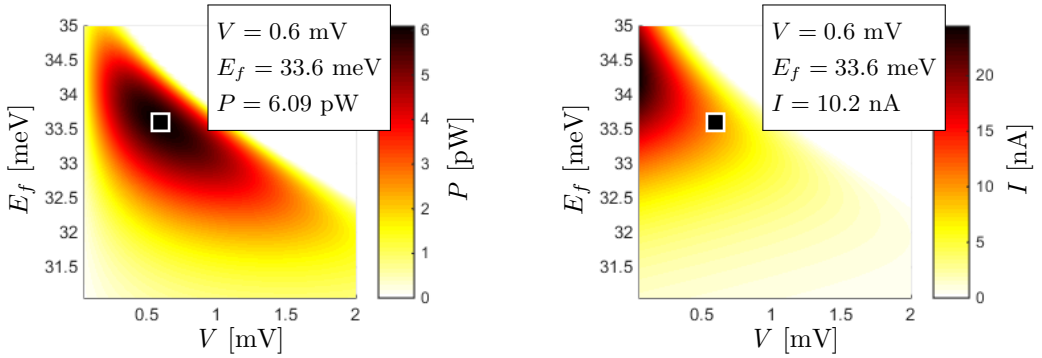

(A) Output power. (B) Current.

FIGURE 3.6.1: 1D output power (A) and current at maximum output power (B) for transport above the barriers in the cold regime.

If we now calculate the output power density and current density in 3D, and normalize the results so the current at maximum output power is the same as the current at maximum output power in the 1D case, we get the graphs in Fig. 3.6.2.

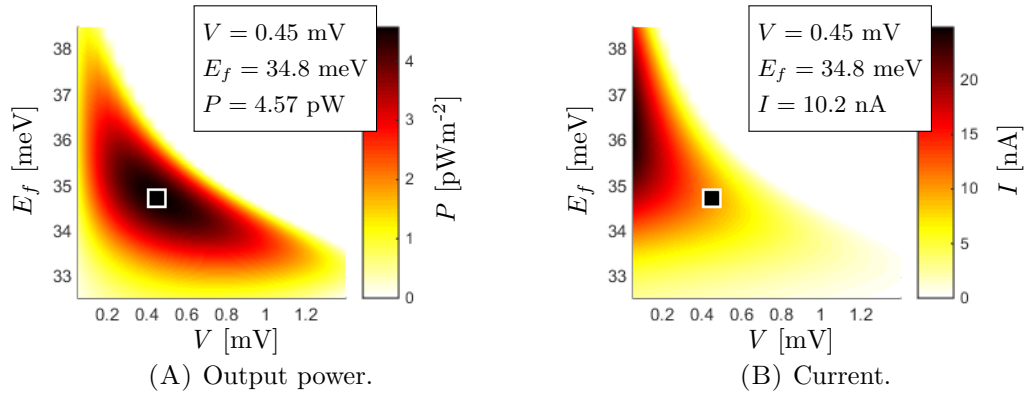

(A) Output power. (B) Current.

FIGURE 3.6.2: Normalized 3D output power (A) and current at maximum output power (B) for transport above the barriers in the cold regime.

We see that, in order to reach the maximum output power in the 3D case, the Fermi level needs to be higher than in the 1D case.

We also see that the maximum output power is a factor 1.33 larger in the 1D case, so it seems indeed like there is something to be gained from using 1D structures in thermoelectric elements. Furthermore, due to additional degrees of freedom for the electrons, the heat current Q should in 3D be larger than in 1D, decreasing the efficiency of the device.

3.6.2 Transport above the barriers - hot temperature regime

We do the same thing in the hot temperature regime, and yield the graphs in Fig. 3.6.3 and 3.6.4.

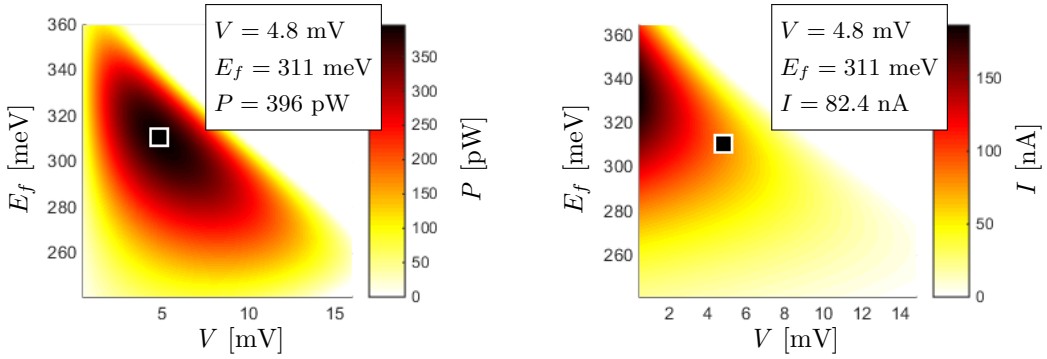

(A) Output power. (B) Current.

FIGURE 3.6.3: 1D output power (A) and current at maximum output power (B) for transport above the barriers in the cold regime.

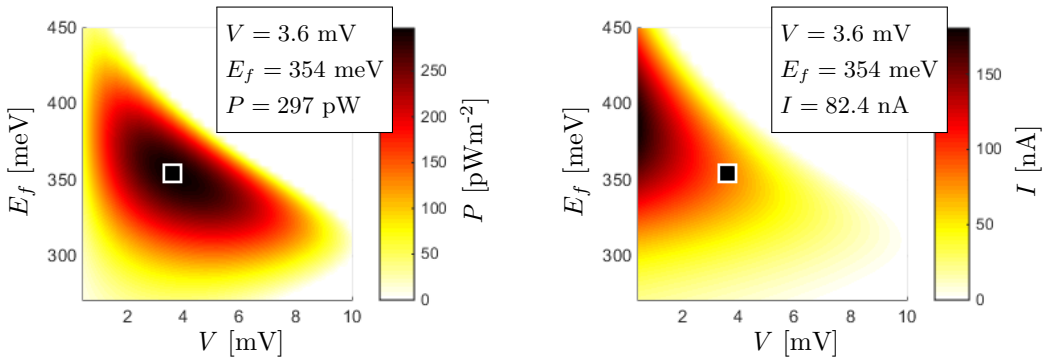

(A) Output power. (B) Current.

FIGURE 3.6.4: Normalized 3D output power (A) and current at maximum output power (B) for transport above the barriers in the cold regime.

The results are the same, and we get the same improvement by a factor of 1.33 in the maximum output power.

Chapter 4

Conclusion

4.1 Transport above the barrier energy

After having investigated how different parameters of the potential structure impacts the transmission function in Sec. 3.1.3, we in Sec. 3.2.1 showed that by using a QD superlattice it is possible to engineer a rectangular transmission band that is wide enough to allow transport of all available electrons from the hot to the cold lead, in order to maximize the output power. The use of a superlattice also enhances the efficiency due to a sharpening of the lower transmission band edge.

When comparing to a single QD yielding the same efficiency, in Sec. 3.3.1, the superlattice structure improves the maximum output power by a factor of 4-4.5.

As shown in Sec. 3.4.1, there is improvement both in maximum output power and efficiency up until a 4 barrier superlattice, after which the output power and efficiency does not change significantly.

4.2 Using antireflection coating

By calculating the transmission function from a QD superlattice structure using antireflection coating, it was in Sec. 3.2.2 showed that it is possible to engineer a very narrow transmission band below the barrier energy, which is expected to maximize the efficiency.

As shown in Sec. 3.3.2 the maximum output power of a superlattice using antireflection coating compared to a single QD with the same efficiency increases by a factor of 40 in the cold regime and 15 in the hot regime. By placing the Fermi level at an appropriate

position and having the proper bias voltage, it is possible to come very close to the maximum Carnot efficiency.

It was also in Sec. 3.4.2 shown that the results do not improve beyond a 4 barrier structure, equivalent to one QD with antireflection coating.

4.3 Asymmetric potential structure

In Sec. 3.5 we showed that transmission functions calculated from potential structures with smaller dimensions are more sensitive to an asymmetric structure. Also, the sensitivity increases as more barriers are added to structure.

4.4 Model limitations

The model we use to calculate the transmission is totally dependent on coherent transport through the obstacle, where all scattering events are elastic. Studies have shown that electrons at temperatures similar to the cold temperature regime we have been using, in similar semiconductor materials, have a coherence length in the hundreds of nanometres [18]. This is also the length of the nanowires modelled in this work, so it is hard to say if the transport in the structures used will remain coherent. Coherence at this temperature is shown to be limited by interface roughness, which is not part of our model. The coherence length decreases with temperature, but a larger temperature also requires smaller superlattice dimensions, so results in the hot temperature regime are also hard to foretell. Since the device performance remains relatively constant when using structures with more than 4 barriers, the type of structures modelled could in fact enable experimental testing of the limits of coherence, since a loss of coherence would lead to a degrading performance.

Models using energy level tunnel couplings and Coulomb interactions are frequently used. These take into account electron-electron interaction and predicts results that have been confirmed experimentally [19]. The model used in this work neglects interactions between electrons, and would also be very hard to implement into the model.

The model lacks a way of calculating the phonon transport, which accounts for a large part of the heat loss. The results for efficiency should for this reason be considered as maximum values. But the result that superlattices have the potential to beat single quantum dots in terms of efficiency still holds. If anything the improvements should in practice be even greater, as a higher number of barriers increases the phonon scattering [20], preventing some of the heat loss.

We choose to limit ourselves to the lowest sub-band. This approximation only holds if the nanowires are extremely thin or the temperatures very low. Adding more sub-bands into the model would certainly have an impact on the results, but it is hard to say in what way.

4.5 Outlook

There are many things, such as phonon transport, contact reflectance and more sub-bands, that could be added to the model in order to make it more realistic. We have only looked at these devices as heat engines, and it would be interesting to model them also as refrigerators. Since systems dependent on quantum mechanics seem to work best at very low temperatures, where thermal effects are small, maybe this would have more relevance from a device point of view. But what would be really interesting is to fabricate an actual device and experimentally test its thermoelectric properties, in order to see to what extent the used model predicts the results.

I am certain thermoelectrics will play its role in the future, one way or the other. If low dimensional superlattices is the way to go remains to be seen.

Bibliography

[1] Thomas Johann Seebeck. *Magnetische Polarisation der Metalle und Erze durch Temperatur-Differenz*. Engelmann, Leipzig, 1895.

[2] Enn Velmre. Proceedings of the estonian academy of sciences: Engineering. In *Thomas Johann Seebeck (1770–1831)*, volume 13, page 276, 2007.

[3] Lon E. Bell. Cooling, heating, generating power, and recovering waste heat with thermoelectric systems. *Science*, 321(5895):1457–61, 2008.

[4] Lon E. Bell, Dwain J. Reed, and Alan D. Miller. Thermoelectric peltier device for local cortical cooling. *Physiology & Behavior*, 20(2):209–11, 1978.

[5] L. D. Hicks and M. S. Dresselhaus. Thermoelectric figure of merit of a one-dimensional conductor. *Physical Review B: Condensed Matter And Material Physics*, 47(24):16631–4, 1993.

[6] Phillip M. Wu. Large thermoelectric power factor enhancement observed in InAs nanowires. *Nano Letters*, 13(9), 2013.

[7] Mattias Jeppsson et al. GaAs/GaSb nanowire heterostructures grown by MOVPE. *Journal Of Crystal Growth*, 310(18):4115–21, 2008.

[8] Zhaoxia Bi et al. InN quantum dots on GaN nanowires grown by MOVPE. *Physica Status Solidi. C : Current Topics In Solid State Physics*, 11(3–4):421–4, 2014.

[9] Robert S. Whitney. Finding the quantum thermoelectric with maximal efficiency and minimal entropy production at given power output. *Physical Review B: Condensed Matter And Material Physics*, 91(11), 2015.

[10] T. C. Harman, P. J. Taylor, D. L. Spears, and M. P. Walsh. Thermoelectric quantum-dot superlattices with high ZT. *Journal of Electronic Materials*, 29(1): L1–4, 2000.

[11] Akshay Agarwal and Bhaskaran Muralidharan. Power and efficiency analysis of a realistic resonant tunneling diode thermoelectric. *Applied Physics Letters*, 105(1), 2014.

[12] Rafael Sanchez and Markus Büttiker. Optimal energy quanta to current conversion. *Physical Review B: Condensed Matter And Material Physics*, 83(8), 2011.

[13] Yu-Ming Lin and M. S. Dresselhaus. Thermoelectric properties of superlattice nanowires. *Physical Review B: Condensed Matter And Material Physics*, 68(7), 2003.

[14] John H. Davies. *The Physics of Low-Dimensional Semiconductors.* Cambridge University Press, 6 edition, 2006.

[15] G. D. Mahan and J. O. Sofo. The best thermoelectric. *Proceedings Of The National Academy Of Sciences Of The United States Of America*, 93(15):7436–9, 1996.

[16] C. Pacher et al. Antireflection coating for miniband transport and Fabry-Pérot resonances in GaAs/AlGaAs superlattices. *Applied Physics Letters*, 79(10):1486–8, 2001.

[17] Rama Venkatasubramanian, Edward Siivola, Thomas Colpitts, and Brooks O'Quinn. Thin-film thermoelectric devices with high room-temperature figures of merit. *Nature*, 413(6856):597–602, 2001.

[18] C. Rauch et al. Transition between coherent and incoherent electron transport in GaAs/GaAlAs superlattices. *Physical Review Letters*, 81(16):3495–8, 1998.

[19] C. Fasth, A. Fuhrer, L. Samuelson, Vitaly N. Golovach, and Daniel Loss. Direct measurement of the spin-orbit interaction in a two-electron InAs nanowire quantum dot. *Physical Review Letters*, 98(26), 2007.

[20] Hiroyuki Sakaki. Quantum wire superlattices and coupled quantum box arrays: A novel method to suppress optical phonon scattering in semiconductors. *Japanese Journal Of Applied Physics*, 28(2):L314–6, 1989.